https://doi.org/10.1093/plcell/koac251 THE PLANT CELL 2022: 34: 4531–4553

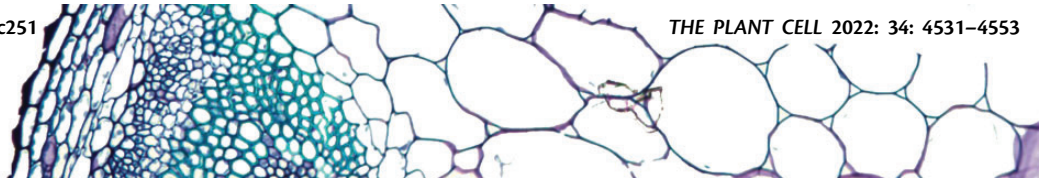

Research Article

Type one protein phosphatase regulates fixed-carbon starvation-induced autophagy in Arabidopsis

Qiuling Wang [1], Qianqian Qin [1], Meifei Su [1], Na Li [1], Jing Zhang [1], Yang Liu [1], Longfeng Yan [1] and Suiwen Hou [1,*]

1 Key Laboratory of Cell Activities and Stress Adaptations, Ministry of Education, School of Life Sciences, Lanzhou University, Lanzhou 730000, People's Republic of China

*Author for correspondence: housw@lzu.edu.cn
These authors contributed equally (Q.W. and Q.Q.).
S.H. and Q.W. designed the research; Q.W., Q.Q., M.S., N.L., J.Z., and Y.L. carried out the experiments; S.H. and Q.W. wrote the manuscript. Q.W. and Q.Q. have contributed equally to this work.
The author responsible for distribution of materials integral to the findings presented in this article in accordance with the policy described in the Instructions for Authors (https://academic.oup.com/plcell) is: Suiwen Hou (housw@lzu.edu.cn).

Abstract

Autophagy, a conserved pathway that carries out the bulk degradation of cytoplasmic material in eukaryotic cells, is critical for plant physiology and development. This process is tightly regulated by ATG13, a core component of the ATG1 kinase complex, which initiates autophagy. Although ATG13 is known to be dephosphorylated immediately after nutrient starvation, the phosphatase regulating this process is poorly understood. Here, we determined that the Arabidopsis (*Arabidopsis thaliana*) septuple mutant (*topp-7m*) and octuple mutant (*topp-8m*) of TYPE ONE PROTEIN PHOSPHATASE (TOPP) exhibited significantly reduced tolerance to fixed-carbon (C) starvation due to compromised autophagy activity. Genetic analysis placed TOPP upstream of autophagy. Interestingly, ATG13a was found to be an interactor of TOPP. TOPP directly dephosphorylated ATG13a in vitro and in vivo. We identified 18 phosphorylation sites in ATG13a by LC-MS. Phospho-dead ATG13a at these 18 sites significantly promoted autophagy and increased the tolerance of the *atg13ab* mutant to fixed-C starvation. The dephosphorylation of ATG13a facilitated ATG1a-ATG13a complex formation. Consistently, the recruitment of ATG13a for ATG1a was markedly inhibited in *topp-7m-1*. Finally, TOPP-controlled dephosphorylation of ATG13a boosted ATG1a phosphorylation. Taken together, our study reveals the crucial role of TOPP in regulating autophagy by stimulating the formation of the ATG1a-ATG13a complex by dephosphorylating ATG13a in Arabidopsis.

Introduction

Autophagy is a conserved biological process in which eukaryotic cells recycle damaged or unwanted cellular components in double-membrane vesicles termed autophagosomes to maintain cellular homeostasis (Michaeli et al., 2016; Marshall and Vierstra, 2018). Autophagy is implicated in almost every aspect of plant life, including development, reproduction, metabolism, and stress tolerance (Doelling et al., 2002; Hanaoka et al., 2002; Ren et al., 2014; Li et al., 2019; Sedaghatmehr et al., 2019; Rodriguez et al., 2020; Zhao et al., 2020).

Autophagy is mainly driven by autophagy-related (ATG) proteins. Numerous ATGs have been discovered in plants over the past few decades (Liu and Bassham, 2012). Proteins that are essential for the autophagic process predominately assemble into several functional complexes: (1) the ATG1 kinase or ATG1-ATG13 complex, which initiates autophagy by responding to changes in nutritional status; (2) the ATG9

Received February 22, 2022. Accepted August 04, 2022. Advance access publication August 12, 2022

IN A NUTSHELL

Background: Autophagy is a conserved, essential degradation process in eukaryotes. This process is mainly driven by numerous autophagy-related (ATG) proteins. Among these components, the ATG1-ATG13 complex plays an essential role in initiating autophagy and the core subunit ATG13 recruits downstream ATG proteins to the ATG1-ATG13 complex. Arabidopsis ATG13 is hyperphosphorylated under nutrient-rich conditions but is dephosphorylated immediately after nutrient starvation.

Questions: Which phosphatase dephosphorylates ATG13? Which components in the autophagy pathway are regulated by TYPE ONE PROTEIN PHOSPHATASE (TOPP)? What is the key phosphorylation site of ATG13a? How does ATG13a phosphorylation regulate autophagy?

Findings: Using T-DNA insertional and CRISPR/Cas9-mediated mutagenesis, we generated septuple (*topp-7m*) and octuple (*topp-8m*) mutants of *TOPP* and demonstrated that these mutants showed a significant autophagy-deficient phenotype upon fixed-carbon starvation. ATG13a was a substrate of TOPP and liquid chromatography/mass spectrometry–mass spectrometry identified 18 phosphorylation sites in ATG13a. Moreover, dephosphorylation of ATG13a by TOPP facilitated ATG1a-ATG13a complex formation to promote autophagy and increase plant tolerance to fixed-carbon starvation.

Next steps: After fixed-carbon starvation, TOPP is activated to dephosphorylate ATG13a. However, how TOPP is activated remains to be determined. In addition, ATG13a contains more than the eighteen phosphorylation sites we identified; how these phosphorylation sites respond to different environmental conditions and nutrient deficiencies requires further study.

cycling system complex, which helps supply the membrane during phagophore expansion; (3) the class III phosphatidylinositol (PI) the 3-kinase (PI3K-III) complex, which mediates vesicle nucleation; (4) two ubiquitin-like conjugation systems (ATG8-PE and ATG5-ATG12), which regulate autophagosome expansion and maturation; and (5) the soluble NSF (N-ethylmaleimide sensitive factor) attachment protein receptor (SNARE) complex, which mediates the fusion of autophagosomes with the vacuole, thus degrading nonfunctional cytoplasmic components (Liu and Bassham, 2012; Marshall and Vierstra, 2018). Among these, the activation of the ATG1-ATG13 complex is the most upstream step of autophagosome formation (Mizushima, 2010). The function of the ATG1-ATG13 kinase complex in plants has gained increasing attention in recent years (Wang and Hou, 2022). Therefore, a complete understanding of this complex is essential for fully elucidating the mechanisms that regulate autophagy.

Studies in yeast (*Saccharomyces cerevisiae*) and vertebrates (*Homo sapiens* or *Mus musculus*) have demonstrated that phosphorylation events play vital roles in the initiation phase of autophagy by regulating the assembly and activity of the Atg1/ULK (Unc-51-like kinase) kinase complex (Xie et al., 2015). The yeast Atg1 kinase complex is composed of the Ser/Thr kinase Atg1, the adaptor protein Atg13, and the ternary complex of Atg17-Atg31-Atg29 (Suzuki et al., 2007; Suzuki and Ohsumi, 2010). Target of rapamycin complex 1 (TORC1) and cAMP-dependent protein kinase (PKA) phosphorylate Atg13 under nutrient-sufficient conditions, preventing autophagy by inhibiting the Atg1-Atg13 interaction (Kamada et al., 2000; Stephan et al., 2009). Inactivation of TORC1 results in Atg13 dephosphorylation, leading to the formation of the Atg1-Atg13-Atg17 complex, which functions in the induction of autophagy (Kamada et al., 2000; Kabeya et al., 2005). Protein phosphatase 2A (PP2A) antagonizes Atg13 phosphorylation and promotes autophagy following the inactivation of TORC1 in yeast (Yeasmin et al., 2016). In addition, the PP2C protein phosphatases Ptc2 and Ptc3 in yeast promote DNA damage- and rapamycin-induced autophagy by dephosphorylating Atg1 and Atg13 (Memisoglu et al., 2019; Memisoglu and Haber, 2019). In mammals, the ULK complex consists of ULK1/2, ATG13, FIP200 (focal adhesion kinase family interacting protein of 200 kDa), and ATG101. Under nutrient-rich conditions, mammalian TORC1 (mTORC1) represses autophagy by directly phosphorylating ULK1 and ATG13 (Chang and Neufeld, 2009; Mizushima, 2010). Inhibiting mTORC1 resulted in increased PP2A activity towards ULK1, thus activating autophagy (Alers et al., 2011; Wong, 2015). Meanwhile, the expression of unphosphorylated ATG13 bypassed the TORC1 pathway to directly induce autophagy in vegetative cells (Puente et al., 2016).

Although the mechanism regulating the phosphorylation of the Atg1-Atg13 complex in yeast and mammals has been largely elucidated, it is not well-defined in plants. In Arabidopsis (*A. thaliana*), the ATG1 kinase complex includes the Ser/Thr kinase ATG1 and its accessory proteins ATG13, ATG11, and ATG101. Plants lacking ATG1, ATG13, or ATG11 are hypersensitive to nutrient limitation and senesce prematurely due to repressed autophagy, suggesting these components are indispensable regulators of plant autophagy (Suttangkakul et al., 2011; Li et al., 2014; Huang et al., 2019; Qi et al., 2019). Nutrient starvation can alter the phosphorylation status of the ATG1-ATG13 complex (Suttangkakul

et al., 2011; Li et al., 2014). Several upstream kinases affecting the activity of the complex have been identified. Overexpressing *TOR* inhibited autophagy in Arabidopsis (Pu et al., 2017), while disrupting TOR continuously activated autophagy (Schumacher et al., 2010; Soto-Burgos and Bassham, 2017). The REGULATORY ASSOCIATED PROTEIN OF mTOR (RAPTOR) interacts with ATG13a via its TOS motif to regulate autophagy (Son et al., 2018). Thus, TOR kinase may be involved in the phosphorylation of the ATG1-ATG13 complex (Van Leene et al., 2019). SNF1 (SUCROSE NONFERMENTING1) KINASE HOMOLOG 10 (KIN10, also known as SnRK1.1) is another kinase implicated in the regulation of the ATG1-ATG13 complex (Chen et al., 2017). Additionally, ATG13a may be a target/substrate of MITOGEN-ACTIVATED PROTEIN KINASE 3 (MPK3) and MPK6 (Hoehenwarter et al., 2013). However, little is known about the phosphatases responsible for the reversal of ATG13 phosphorylation in plants. Moreover, the phosphorylation sites of ATG13 and the downstream events regulated by its phosphorylation are poorly understood.

Plants express a variety of protein phosphatases (PP), including PP1, PP2A, PP2C, PP4, and PP6. Among these, PP1 plays an important role in regulating plant growth, development, and stress responses (Bheri et al., 2021). There are nine isoforms of PP1 in Arabidopsis, which are referred to as TYPE ONE PROTEIN PHOSPHATASEs (TOPPs). TOPP enzymes regulate the DELLA-mediated gibberellin signaling pathway (Qin et al., 2014), phytochrome B-mediated hypocotyl elongation (Yue et al., 2016), PIN-FORMED 1 (PIN1) polarity and trafficking (Guo et al., 2015), plant immunity (Liu et al., 2019; Yan et al., 2019; Hu et al., 2022), abscisic acid signaling (Hou et al., 2016; Zhang et al., 2020; Hu et al., 2022), and cell wall integrity during tip-growth of pollen tubes and root hairs (Franck et al., 2018). In addition, OsPP1a and TdPP1a might function in the salt stress response in rice (*Oryza sativa*) and wheat (*Triticum aestivum*), respectively (Liao et al., 2016; Bradai et al., 2018). TdPP1 participates in brassinosteroid-mediated control of root growth via the activation of BRI1-EMS SUPPRESSOR 1 (BES1; Bradai et al., 2021). GmTOPP13 is involved in drought tolerance in soybean (*Glycine max*; Wang et al., 2021). In the current study, we determined that TOPP, a regulator of the ATG1-ATG13 complex in Arabidopsis, promotes autophagy by dephosphorylating ATG13a and modulating the formation of the ATG1a-ATG13a complex under fixed-carbon (C) starvation, shedding light on the role of a protein phosphatase in this crucial process in plants.

Results

Plants lacking at least seven members of TOPP are hypersensitive to fixed-C starvation

Autophagy-defective mutants are characterized by hypersensitivity to fixed-C deprivation (Doelling et al., 2002; Hanaoka et al., 2002; Yoshimoto et al., 2004; Chung et al., 2010; Suttangkakul et al., 2011; Huang et al., 2019; Qi et al., 2019; Liu et al., 2020). We previously determined that the dominant-negative Arabidopsis mutant *topp4-1* (Qin et al., 2014) displayed early senescence after fixed-C starvation, similar to autophagy-defective mutants (Supplemental Figure S1, A and B). Overexpression of *TOPP4* partially inhibited premature senescence in *topp4-1*, indicating that this phenotype of *topp4-1* is caused by the loss function of TOPP4. However, no obvious phenotype was observed in the *TOPP4* T-DNA insertion mutant *topp4-3* (Supplemental Figure S1, A and B).

To gain further insight into the role of *TOPP* in carbon deprivation, we first analyzed the transcript levels of *TOPPs* after fixed-C starvation by performing RT-qPCR. The expression of *TOPPs* was induced after treatment (Supplemental Figure S2), suggesting that there may be functional redundancy among *TOPPs* in response to fixed-C starvation. We then identified or generated all single mutants of the *TOPP* family (Supplemental Figure S3, A and B). However, all of the homozygous *TOPP* single mutants appeared similar to the wild type (WT) in response to fixed-C starvation (Supplemental Figure S4). We subsequently generated the *topp-2m* (*topp1 topp4* [*topp1/4*], *topp6 topp7* [*topp6/7*], *topp8 topp9* [*topp8/9*]), *topp-3m* (*topp1 topp2 topp4* [*topp1/2/4*], *topp3 topp6 topp7* [*topp3/6/7*], *topp1 topp4 topp5* [*topp1/4/5*], *topp6 topp7 topp9* [*topp6/7/9*]), *topp-4m* (*topp1 topp4 topp6 topp7* [*topp1/4/6/7*], *topp2 topp6 topp7 topp9* [*topp2/6/7/9*], *topp4 topp6 topp7 topp9* [*topp4/6/7/9*]), *topp-5m* (*topp1 topp4 topp6 topp7 topp9* [*topp1/4/6/7/9*]), and *topp-6m* (*topp1 topp2 topp4 topp6 topp7 topp9* [*topp1/2/4/6/7/9*]) mutants (Supplemental Figure S3, B and C and Supplemental Data Set S1). Unfortunately, none of these mutants displayed obvious phenotypes under fixed-C starvation conditions compared to WT (Supplemental Figure S5).

We then performed CRISPR-Cas9-mediated gene editing by cloning gRNA targets for *TOPP5* and *TOPP8* into pHEE401 and subsequently transforming *topp-5m* (*topp1/4/6/7/9*) with this construct to generate the septuple mutant *topp-7m-1* (*topp1 topp4 topp5 topp6 topp7 topp8 topp9* [*topp1/4/5/6/7/8/9*]), as reported previously (Liu et al., 2019; Zhang et al., 2020; Figure 1A; Supplemental Figure S3C). Under fixed-C starvation, *topp-7m-1* exhibited an early senescence phenotype, similar to that observed for *topp4-1* (Figure 1, B and E). This phenotype was rescued by expressing *TOPP1*, *TOPP4*, *TOPP5*, *TOPP8*, and *TOPP9* driven by their native promoters in the *topp-7m-1* #79 background (refers to line #79 hereafter; Figure 1, C and F; Supplemental Figure S6). However, *TOPP7* failed to fully complement *topp-7m-1* (Supplemental Figure S6, B and D). We generated *topp-7m-2* (*topp1 topp2 topp4 topp6 topp7 topp8 topp9* [*topp1/2/4/6/7/8/9*]), *topp-7m-3* (*topp1 topp2 topp4 topp5 topp6 topp7 topp9* [*topp1/2/4/5/6/7/9*]), and the octuple mutant *topp-8m* (*topp1 topp2 topp4 topp5 topp6 topp7 topp8 topp9* [*topp1/2/4/5/6/7/8/9*]) by crossing *topp-7m-1* with *topp-6m* (*topp1/2/4/6/7/9*; Figure 1A; Supplemental Figure S3C). Similar to *topp-7m-1*, *topp-7m-2* and *topp-7m-3* were extremely sensitive to fixed-C starvation (Supplemental Figure S1, C and D), as was *topp-8m* (Figure 1, B and E).

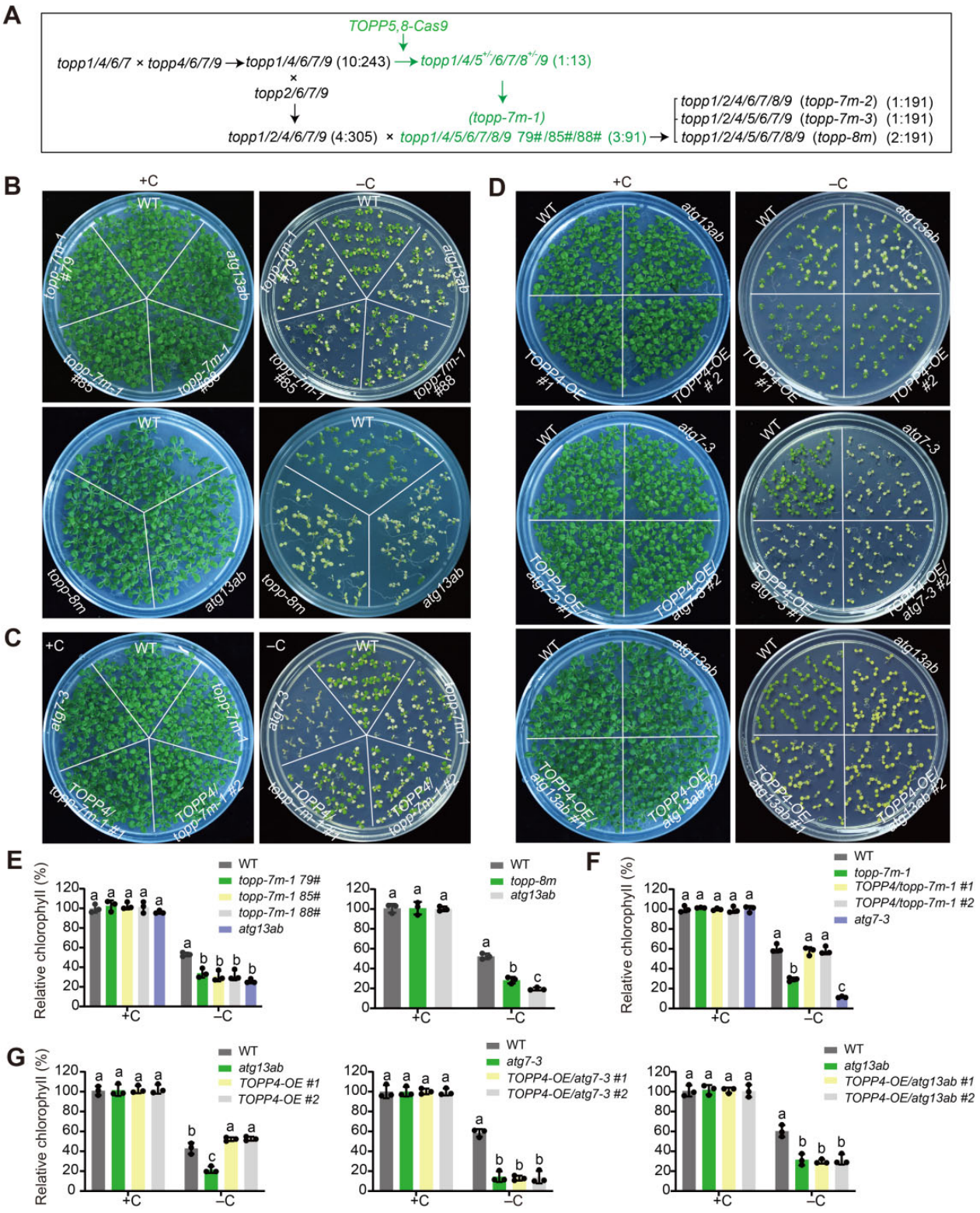

Figure 1 Plants lacking at least seven members of TOPP are hypersensitive to fixed-C starvation. A, Generation of *topp* septuple mutants (*topp-7m*) and octuple mutants (*topp-8m*). To generate *topp-7m-1* (*topp1/4/5/6/7/8/9*), two sgRNAs targeting *TOPP5* and *TOPP8* were designed to create *topp-7m-1* mutants in the background of the quintuple mutant *topp1/4/6/7/9*; #79, #85, and #88 refer to different editing lines of *topp-7m-1*, and all *topp-7m-1* in the following text indicates line #79. To generate *topp-7m-2* (*topp1/2/4/6/7/8/9*), *topp-7m-3* (*topp1/2/4/5/6/7/9*), and *topp-8m* (*topp1/2/4/5/6/7/8/9*), *topp-7m-1* was crossed with the sextuple mutant *topp1/2/4/6/7/9*. "×" indicates crossing. Numbers in brackets represent the progeny frequencies from the F_2 generation or T_1/T_2 transgenic lines. B, Phenotypes of *topp-7m-1* and *topp-8m* in response to fixed-C starvation. WT, *topp-7m-1*, *topp-8m*, and *atg13ab* seedlings grown on 1/2 MS solid medium with sucrose under long day (LD; 16 h light/8 h dark) conditions continuously (+ C), or grown on sucrose-free 1/2 MS solid medium under LD for 7 d, placed in the dark for 9–10 d, and allowed to

(continued)

Together, these results suggest that *TOPPs* function redundantly in fixed-C starvation-induced senescence.

By contrast, *TOPP1*, *TOPP4*, and *TOPP5* overexpression lines displayed higher tolerance to fixed-C starvation than WT (Figure 1, D and G; Supplemental Figure S7). To understand the genetic relationship between *TOPP* and autophagy-dependent genes, we overexpressed *TOPP4* in the *atg7-3* and *atg13ab* mutant backgrounds. Interestingly, *atg7-3* and *atg13ab* plants harboring *35S:TOPP4-GFP* displayed similar sensitivity to fixed-C starvation compared to the *atg7-3* and *atg13ab* mutants (Figure 1D). This was further supported by the decreased relative chlorophyll content in these lines vs. WT under fixed-C starvation conditions (Figure 1G). These results indicate that the enhanced tolerance to fixed-C starvation in the *TOPP4-OE* lines is dependent on the autophagy pathway.

Fixed-C starvation-induced autophagy is repressed in the absence of TOPP

To further address the role of TOPP in fixed-C starvation-induced autophagy, we treated the plants with calyculin A (CL-A), a pharmacological inhibitor of the protein phosphatases PP2A and PP1 (Stubbs et al., 2001; Wright et al., 2002; Takahashi et al., 2012). In the presence of concanamycin A (ConcA), an autophagy inhibitor that stabilizes autophagic bodies (Yoshimoto et al., 2004; Thompson et al., 2005; Phillips et al., 2008; Chung et al., 2010), the fixed-C starvation-induced translocation of GFP-ATG8e, YFP-ATG1a, and YFP-ATG13a labeled vesicles was strongly enhanced, as previously reported. However, upon CL-A treatment, this translocation was significantly reduced (Supplemental Figure S8, A and B). These findings suggest that phosphatase activity is required for fixed-C starvation-induced autophagy.

Autophagy-deficient mutants exhibit premature senescence due to inhibited autophagosome formation. To investigate whether inhibiting TOPP activity reduces the formation of autophagosomes, we expressed YFP-ATG8e, YFP-ATG1a, and YFP-ATG13a driven by the *35S* promoter in WT and *topp-7m-1* plants. The formation of YFP-labeled puncta structures was more significantly reduced in *topp-7m-1* than in WT after fixed-C starvation (Figure 2, A and B). We then used the release of free YFP from YFP-ATG8e to monitor autophagic transport, as previously reported (Chung et al., 2010). Consistent with the microscopy results, free YFP levels were substantially reduced in *topp-7m-1* upon fixed-C starvation (Figure 2C). Since ATG1 and ATG13 are substrates of autophagy whose levels are elevated in various *atg* mutants (Suttangkakul et al., 2011), we examined the levels of these proteins in *topp-7m-1* after fixed-C starvation using specific antibodies. Immunoblotting analysis revealed stronger accumulation of ATG1a and ATG13a in *topp-7m-1* than in WT (Figure 2D). We also checked the autophagy flux in *topp4-1*, and similar results were obtained (Supplemental Figure S8, C–F). These data demonstrate that TOPP plays an important role in autophagy.

TOPP directly interacts with ATG13a and associates with autophagosomes

To understand the role of TOPP in regulating autophagy, we first analyzed the transcript levels of *ATGs* in WT and *topp-7m-1* plants following fixed-C starvation via RT-qPCR analysis. The transcript levels of *ATG1a*, *ATG13a*, *ATG8a*, *ATG8e*, *ATG5*, and *ATG7* were similar in the mutant and WT (Supplemental Figure S9), suggesting that TOPP does not regulate autophagy at the transcriptional level. We then performed liquid chromatography-tandem mass spectrometry (LC-MS/MS) to analyze the proteins that coimmunoprecipitated with TOPP4-GFP in a coimmunoprecipitation (Co-IP) assay. One candidate protein that we identified was ATG13a, comprising three specific peptides (Supplemental Table S1). Yeast two-hybrid (Y2H) and pull-down assays indicated that TOPP4 physically interacts with ATG13a (Figure 3, A and B). Bimolecular fluorescence complementation (BiFC) assays further confirmed their interaction in vivo (Figure 3D).

We then examined the interactions between TOPP family proteins and ATG13a by performing Y2H and BiFC assays. Besides TOPP4, TOPP1 and TOPP5 also directly interacted with ATG13a (Figure 3A). All nine TOPP proteins interacted with ATG13a in BiFC experiments in *Nicotiana benthamiana* (Figure 3D). To further confirm their interactions in Arabidopsis, we performed a Co-IP assay. TOPP4 was coimmunoprecipitated with ATG13a, and this interaction was enhanced by fixed-C starvation (Figure 3E). Similar results were also obtained for TOPP1 and TOPP5 (Supplemental Figure S10A). ATG13b is another homologous protein of ATG13a; these proteins play redundant roles in the biogenesis of autophagy (Suttangkakul et al., 2011). However, no interaction was detected between TOPPs and ATG13b in Y2H, pull-down, or BiFC assays (Figure 3, A and C; Supplemental Figure S10B). We then examined whether the interaction between ATG13b and TOPPs is induced by autophagy in Arabidopsis. In the Co-IP assay, although it was difficult to detect the interaction between ATG13b and TOPP4 under nutrient-rich conditions, significantly enhanced interaction signals were observed after the induction

Figure 1 (Continued)
recover for 3–4 d in LD (−C). C, *TOPP4* recovers the sensitivity of *topp-7m-1* to fixed-C starvation. One-week-old WT, *pTOPP4:TOPP4-GFP/topp-7m-1*, and *atg7-3* seedlings were treated the same as in (B). D, Enhanced tolerance of the *TOPP4-OE* lines to fixed-C starvation is dependent on the autophagy pathway. One-week-old WT, *p35S:TOPP4-GFP*/WT, *p35S:TOPP4-GFP/atg7-3*, and *p35S:TOPP4-GFP/atg13ab* seedlings were treated the same as in (B). E–G, Relative chlorophyll contents of the seedlings with or without fixed-C starvation shown in (B–D). The relative chlorophyll contents were calculated by comparing the values in −C versus + C seedlings. Values are means ± SD of three biological replicates. Significant differences were calculated by one-way ANOVA. Different letters above each bar indicate statistically significant differences, as determined by Tukey's multiple testing methods ($P < 0.05$). For each biological replicate, a population of at least 25 plants was examined per genotype.

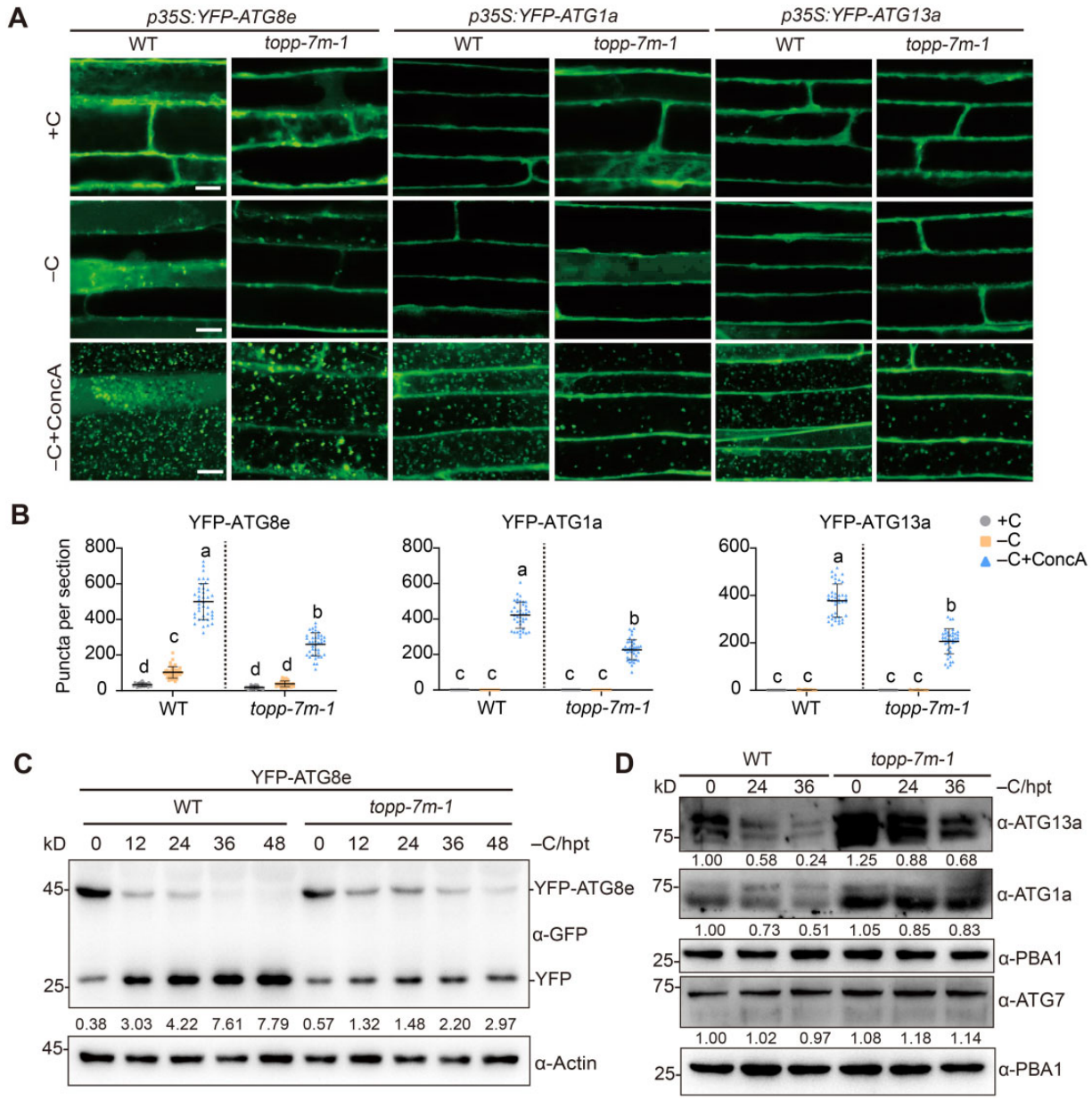

Figure 2 *TOPPs* are required for autophagic turnover. A, Confocal images of YFP-(ATG8e, ATG1a, ATG13a)-labeled autophagic bodies inside the central vacuoles. WT or *topp-7m-1* seedlings expressing *YFP-ATG8e*, *YFP-ATG1a*, and *YFP-ATG13a* grown for 5 d on 1/2 MS solid medium were transferred to fresh 1/2 MS liquid medium (+ C) or sucrose-free 1/2 MS liquid medium and incubated in the dark for 12 h (–C) with or without the addition of 0.5 μM ConcA (Concanamycin A). Scale bars, 10 μm. B, Quantification of the number of autophagic bodies shown in (A). Four different images in the root elongation zone were photographed per seedling, and the number of puncta in each image was counted and averaged. A total of 10 seedlings were observed per treatment. Data represent mean ± SD (n = 40), analyzed by one-way ANOVA followed by Tukey's multiple comparison analyses ($P < 0.05$). The center line represents the mean of autophagic bodies. Whiskers represent two SDs. Different letters represent significantly different means. C, Immunoblotting analysis showing the processing of YFP-ATG8e fusion proteins in WT and *topp-7m-1* after fixed-C starvation. Seedlings were treated with fixed-C starvation for the indicated time. Total proteins were extracted from the samples and analyzed with anti-GFP antibody. Actin was used as a protein loading control. Values below each lane represent the ratio of free YFP to YFP-ATG8e, as quantified by ImageJ. hpt, hours post-treatment. D, ATG1a and ATG13a protein levels in WT and *topp-7m-1*. The relative intensities of each band against the PBA1 loading control were quantified using ImageJ, and the amount in the first lane in each experiment was set to 1. The gray value of two bands of ATG13a or ATG1a was calculated as a whole. ATG7 was used as a control. All experiments were repeated at least 3 times with similar results. hpt, hours post-treatment.

of autophagy by carbon deprivation (Figure 3F). All of these findings demonstrate that ATG13, especially ATG13a, is a potential target of TOPP in Arabidopsis.

To explain how TOPP is involved in fixed-C starvation-induced autophagy, we first examined the localization of TOPP using transgenic Arabidopsis lines expressing TOPP-GFP

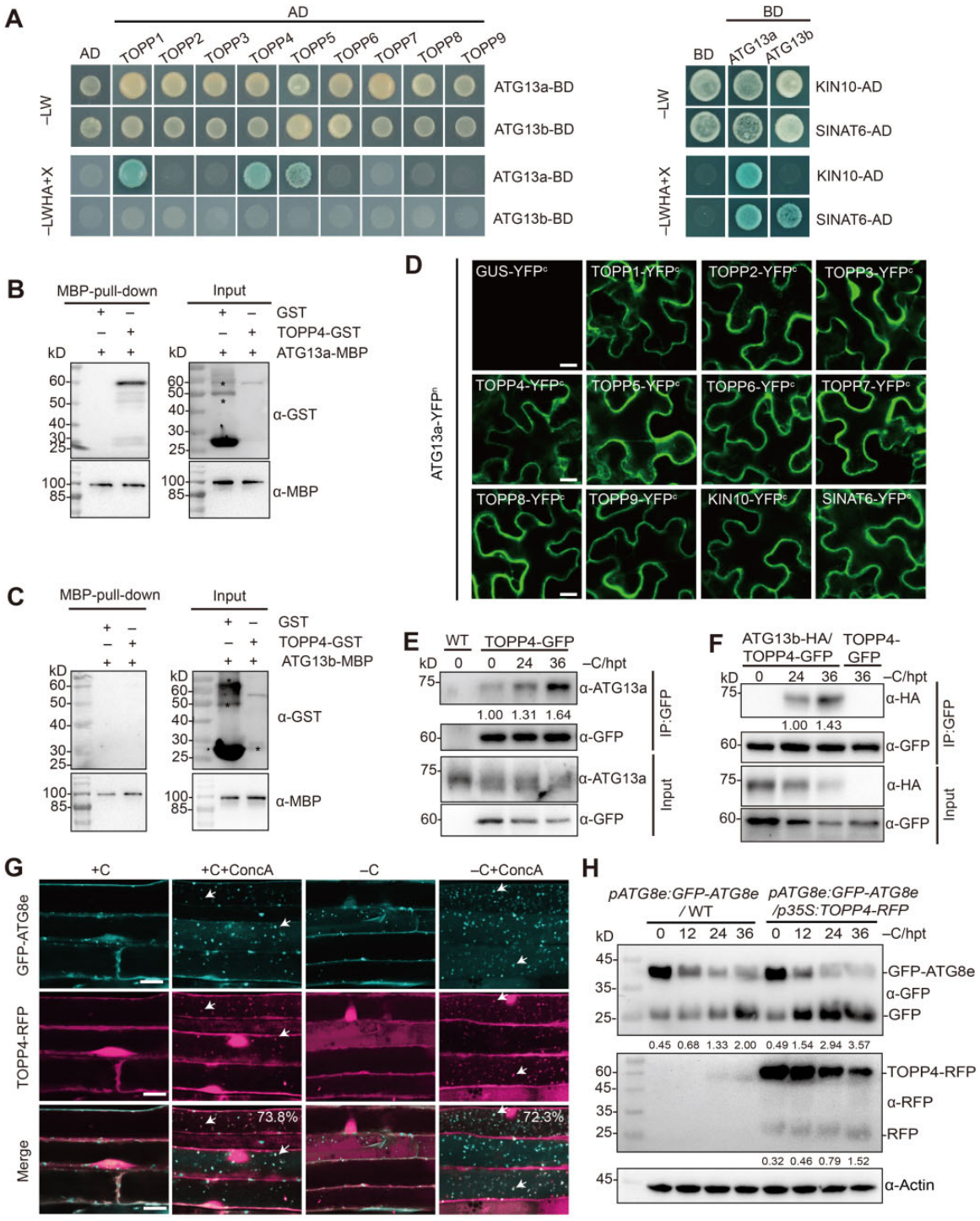

Figure 3 TOPP interacts with ATG13 and associates with autophagosomes. A, Interaction of TOPPs with ATG13a and ATG13b in Y2H assays. –LW, SD medium lacking Trp and Leu; –LWHA + X, SD medium lacking Trp, Leu, His, and Ade; X, X-α-gal. Empty AD, KIN10, and SINAT6 were used as controls. B and C, Pull-down assays showing the interaction of TOPP4 with ATG13a and ATG13b. ATG13a-MBP and ATG13b-MBP were immobilized on MBP Sepharose beads, incubated with GST or TOPP4-GST protein, and subjected to immunoblot analysis with anti-GST antibody. Asterisks represent nonspecific bands. Experiments were repeated twice with similar results. D, BiFC assays showing interactions between TOPPs and ATG13a in *N. benthamiana*. Scale bars, 50 μm. β-glucuronidase (GUS), KIN10, and SINAT6 were used as controls. E and F, Coimmunoprecipitation of TOPP4 with ATG13a and ATG13b in Arabidopsis. For ATG13a, 7-d-old *p35S:TOPP4-GFP*/WT seedlings were treated with fixed-C starvation for 0, 24, and 36 h. Total proteins were immunoprecipitated with GFP magnetic beads and analyzed using anti-ATG13a antibody. WT was used as a negative control. For ATG13b, *pUBQ10:ATG13b-HA*/WT was crossed with *p35S:TOPP4-GFP*/WT. Seven-day-old coexpression lines were treated with fixed-C starvation for the indicated time. Total proteins were immunoprecipitated with GFP magnetic beads and analyzed using anti-HA antibody. *p35S:TOPP4-GFP*/WT was used as a negative control. Values below each lane represent the relative abundance of ATG13a or ATG13a-HA coimmunoprecipitated by TOPP4-GFP, as quantified by ImageJ. hpt, hours post-treatment. G, Intracellular

(continued)

driven by the 35S promoter. Under normal growth conditions, TOPP1, TOPP4, and TOPP5 localized to the cytoplasm and nucleus; this pattern was not altered by fixed-C starvation (Supplemental Figure S11, A and B). However, upon ConcA treatment, TOPP translocated to the vacuole via small vesicles, and many more punctate structures were observed after fixed-C deprivation (Supplemental Figure S11, A and B). Similar results were observed in *pTOPP4:TOPP4-GFP*/WT (Supplemental Figure S11, C and D), indicating that the trafficking of TOPP into vesicle was not the result of its overexpression.

To further confirm these TOPP-labeled puncta structures were related to autophagic vesicles, we crossed *p35S:TOPP4-RFP*/WT with *pATG8e:GFP-ATG8e*/WT, a well-characterized autophagosome marker line (Xiao et al., 2010), and performed confocal microscopy of root cells. A portion (approximately 70%) of TOPP4-RFP colocalized with GFP-ATG8e-decorated autophagic bodies (Figure 3G). Additionally, TOPP4-GFP marked vesicles were almost undetectable in *atg7-3*, and only a few such vesicles were observed in *atg13ab* (Supplemental Figure S11, E and F). Perhaps autophagy is completely blocked in plants lacking the core component ATG7, while residual autophagy still exists in *atg13ab* (Suttangkakul et al., 2011; Li et al., 2014; Huang et al., 2019). These results suggest that TOPP4 puncta are autophagy-dependent.

Given that ATG8 is unstable under acidic conditions and degrades in vacuoles (Yoshimoto et al., 2004; Thompson et al., 2005; Chung et al., 2010) and that TOPP4 enters vacuoles, like ATG8e, we examined the stability of TOPP4 fusion protein under fixed-C starvation. The degradation of TOPP4 was observed, although its level did not decrease as rapidly as that of ATG8e (Figure 3H). By contrast, this degradation was dramatically inhibited in *atg13ab* and *atg7-3* compared to WT (Supplemental Figure S11G). We further found that the degradation of TOPPs was significantly prevented in the presence of the autophagy inhibitor ConcA (Supplemental Figure S11H). These findings indicate that TOPP4 is associated with autophagosomes, which is induced by fixed-C starvation.

TOPP dephosphorylates ATG13a in vitro and in vivo

ATG13a was shown to be a reversibly modified phosphoprotein in Arabidopsis (Suttangkakul et al., 2011). We further confirmed this by performing a dephosphorylation assay using *p35S:YFP-ATG13a*/WT transgenic lines (Supplemental Figure S12, A and B). The band containing ATG13a migrated more quickly due to rapid dephosphorylation upon fixed-C starvation compared to the control, as determined by immunoblotting using anti-phosphoserine (pSer) antibody (Figure 4A). We next examined whether TOPP dephosphorylates ATG13a directly. The recombinant protein TOPP4-GST purified from *E. coli* was confirmed to display phosphatase activity, as it catalyzed the hydrolysis of the general substrate p-nitrophenyl phosphate (pNPP; Figure 4B). After TOPP4-GST treatment, faster migration of ATG13a bands was observed, and this was immediately suppressed by treatment with a protein phosphatase inhibitor (PhosSTOP), suggesting that TOPP4, like λPP (Supplemental Figure S12B), directly dephosphorylates ATG13a in vitro (Figure 4C). Other TOPP family proteins such as TOPP1, TOPP3, and TOPP9, which exhibited phosphatase activity in vitro in our previous study (Zhang et al., 2020), also directly dephosphorylated ATG13a, like TOPP4 (Figure 4D), suggesting that TOPPs redundantly regulate the dephosphorylation of ATG13a.

To further verify the dephosphorylation of ATG13a by TOPP, we coexpressed YFP-ATG13a and TOPP4-RFP in *N. benthamiana* leaves. YFP-ATG13a generated a weaker phosphorylation signal when coexpressed with TOPP4-RFP compared to GUS-RFP (Figure 4E), indicating ATG13a undergoes TOPP4-mediated dephosphorylation in planta. Similar results were obtained using TOPP1, TOPP3, and TOPP9 (Figure 4F). We next investigated the phosphorylation of ATG13a in *topp-7m-1*. After exposure to fixed-C starvation, the ATG13a bands migrated more rapidly in WT plants. However, this trend was impeded in *topp-7m-1*, and ATG13a appeared larger in the mutant (Figure 4, G and H). Similar results were obtained in *topp4-1* (Supplemental Figure S12C). In addition, λPP treatment removed these larger bands of ATG13a (Figure 4H), suggesting that the slow migration of ATG13a in *topp-7m-1* or *topp4-1* was caused by phosphorylation rather than other protein modifications.

To verify these results, we detected immunoprecipitated proteins with pSer antibody. The dephosphorylation of YFP-ATG13a was significantly prevented in *topp-7m-1* (Figure 4I). Since seedlings overexpressing *TOPP* showed increased tolerance to carbon deficiency (Figure 1, D and G; Supplemental Figure S7), we examined the phosphorylation status of ATG13a in *TOPP* overexpression lines. Rapidly migrating bands continuously appeared in the *TOPP-OE* lines compared to the WT (Supplemental Figure S12, D–F). Taken together, these experiments support the notion that ATG13a is the substrate of TOPP and that the autophagy defects in *topp-7m-1* and *topp4-1* might be due to the repression of ATG13a dephosphorylation.

Figure 3 (Continued)
colocalization of TOPP4-RFP with GFP-ATG8e. Five-day-old seedlings coexpressing TOPP4-RFP and GFP-ATG8e grown on 1/2 MS medium were transferred to +C or −C conditions with or without 0.5 μM ConcA for 12 h. The percentages in the merged images indicate the contribution of TOPP4 to the autophagy pathway and were quantified by counting the number of merged puncta to the total number of TOPP4-RFP puncta from 10 images of five plants. Arrows indicate the merged puncta. Scale bars, 10 μm. H, Degradation of GFP-ATG8e and TOPP4-RFP in WT upon fixed-C starvation. One-week-old WT seedlings and *p35S:TOPP4-RFP*/WT seedlings expressing GFP-ATG8e were treated with fixed-C starvation for the indicated time. Total proteins were analyzed by immunoblotting with anti-GFP or -RFP antibody. Values below each lane represent the ratio of free GFP to GFP-ATG8e or free RFP to TOPP4-RFP, as quantified by ImageJ. hpt, hours post-treatment.

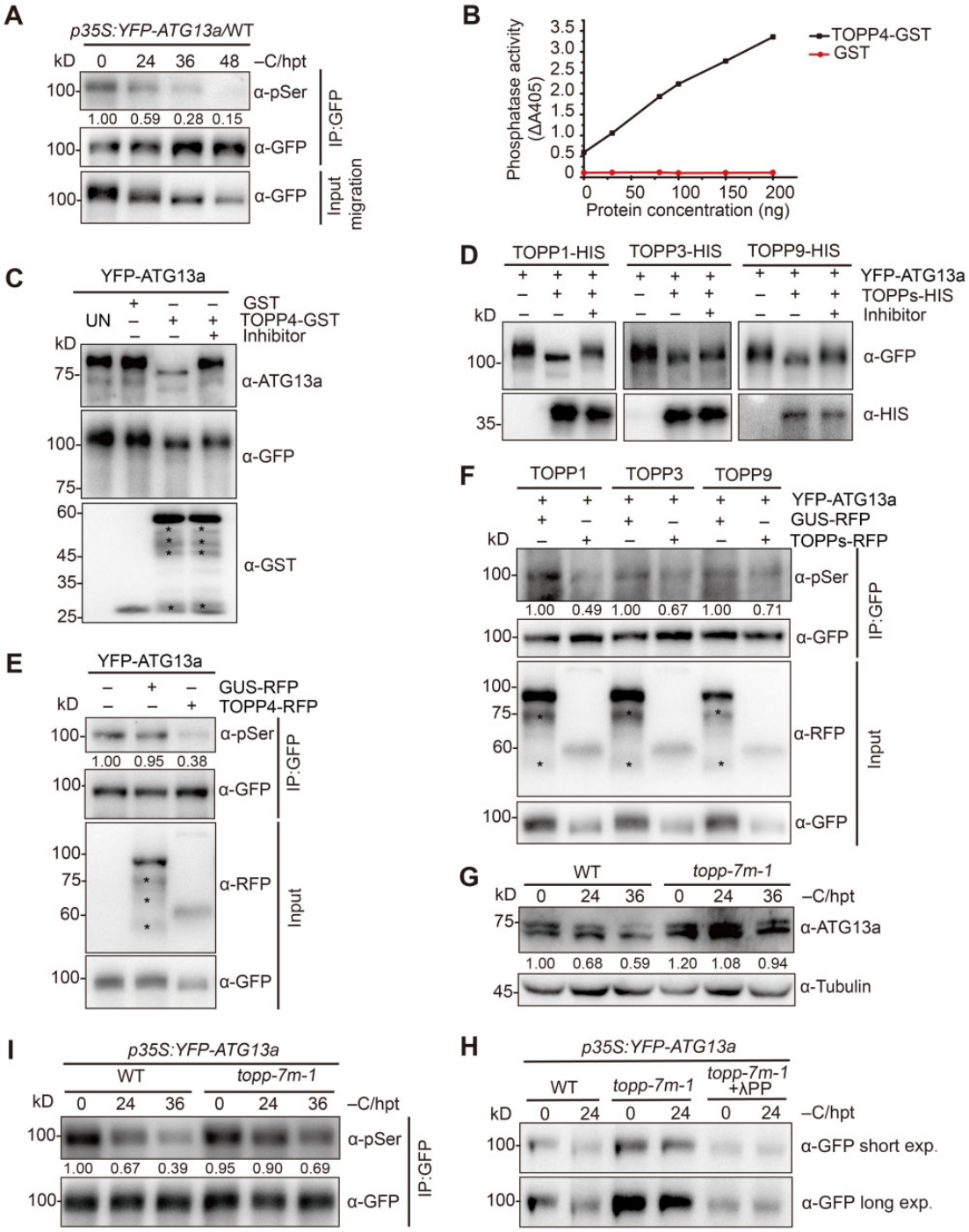

Figure 4 TOPP dephosphorylates ATG13a in vitro and in vivo. A. Fixed-C starvation induces the rapid dephosphorylation of ATG13a. *p35S:YFP-ATG13a*/WT seedlings grown on 1/2 MS medium for 7 d were treated with fixed-C starvation for the indicated time. Phosphorylation of ATG13a was examined by immunoblotting with anti-pSer antibody. Numbers below each lane represent the relative abundance of phosphorylated ATG13a. hpt, hours post-treatment. B, Detection of purified TOPP4-GST enzyme activity in vitro. The phosphatase activity of TOPP4-GST was determined by a colorimetric assay using the substrate p-nitrophenyl phosphate (pNPP). GST was used as a negative control. C, Dephosphorylation of ATG13a by TOPP4-GST. One-week-old *p35S:YFP-ATG13a*/WT seedlings were grown on 1/2 MS medium. Total protein extracts were immunoprecipitated with GFP magnetic beads, treated with TOPP4-GST with or without the phosphatase inhibitor PhosSTOP, and immunoblotted with anti-GFP, -GST, or -ATG13a antibody. UN, untreated extracts. Asterisks represent nonspecific bands. D, Dephosphorylation of ATG13a by TOPP1, TOPP3, and TOPP9 in vitro. Seedlings were treated the same as in (C). Total protein extracts were treated with TOPP1-HIS, TOPP3-HIS, or TOPP9-HIS and subjected to immunoblot analysis with anti-GFP or anti-HIS antibody. E and F, In vivo dephosphorylation of ATG13a by TOPP4, TOPP1, TOPP3, and TOPP9. TOPPs-RFP together with YFP-ATG13a was transiently coexpressed in *N. benthamiana* leaves. Phosphorylation of ATG13a was examined by immunoblotting using anti-pSer antibody. Numbers below the blots represent the relative abundance of phosphorylated ATG13a. Asterisks represent nonspecific bands. GUS-RFP was used as a negative control. G–I, Dephosphorylation of ATG13a in WT and *topp-7m-1* after fixed-C starvation confirmed by immunoblotting with different antibodies. Seedlings were treated the same as in (A). For (G), numbers below the blots represent the abundance of ATG13a. For (I), numbers below the blots indicate the relative abundance of phosphorylated ATG13a. Long exp. and short exp. indicate long and short exposure times. All protein experiments were repeated at least 3 times with similar results. hpt, hours post-treatment.

ATG13a undergoes multi-site phosphorylation

After establishing ATG13a as a substrate of TOPP, we tried to identify the potential phosphorylation sites of ATG13a by enriching YFP-ATG13a protein from transgenic *p35S:YFP-ATG13a*/WT plants grown under normal conditions and analyzing its in vivo phosphorylation sites by LC-MS/MS. At least 11 phosphorylated peptides and 18 unique phosphorylation sites were identified in ATG13a (Figure 5A; Supplemental Data Set S2). Among these, five serine residues (Ser248, Ser397, Ser404, Ser406, and Ser407) were previously reported (Van Leene et al., 2019). We further found that eight of these amino acid residues are also conserved in ATG13b (Supplemental Figure S13). Sequence analysis showed that Ser248, Ser343, Ser397, and Ser473 are highly conserved in different plants, whereas others are specific to Arabidopsis (Supplemental Table S2; Supplemental Figure S14). Additionally, our previous quantitative phosphorylation proteomics analysis (Supplemental Data Set S3) showed that three specific peptides of ATG13a containing the conserved residues Ser248, Ser397, and Ser473 were found in both WT and *topp4-1* (Supplemental Table S3). These results suggest that Ser248, Ser343, Ser397, and S473 affect the function of ATG13a.

To evaluate the contribution of these four conserved phosphorylation sites to fixed-C starvation tolerance, we introduced point mutations (phosphor-dead [S/T/Y to A] or phosphor-mimic [S/T/Y to D]) into the full-length wild-type ATG13a polypeptide and generated transgenic lines expressing these proteins with YFP tag, driven by the 35S promoter, in the *atg13ab* background. However, overexpression of *ATG13a*, *ATG13a*^{4A}, and *ATG13a*^{4D} in the *atg13ab* background completely restored the sensitivity of the mutant to fixed-C starvation (Supplemental Figure S15, A and B). Consistently, similar to ATG13a, both ATG13a^{4A} and ATG13a^{4D} were still sensitive to λPP and TOPP4-GST treatment in vitro (Supplemental Figure S15C). Moreover, when YFP-ATG13a^{4A} or YFP-ATG13a^{4D} was coexpressed with TOPP4-RFP in *N. benthamiana* leaves, the mutated proteins could be still dephosphorylated like the wild-type ATG13a (Supplemental Figure S15D). In addition, the migration caused by the dephosphorylation of ATG13a^{4A} and ATG13a^{4D} after fixed-C starvation was not significantly altered compared with ATG13a (Supplemental Figure S15E). Collectively, these results indicate that the four conserved residues are not sufficient to activate ATG13a and that TOPP dephosphorylates ATG13a at multiple sites during autophagy.

ATG13a dephosphorylation enhances fixed-C starvation-induced autophagy

Given that the substitutions of S248, S343, S397, and S473 had no significant effect on the rescue of *atg13ab*, we reasoned that the activity of ATG13a might be influenced by the number rather than the locations of available phosphorylation sites. To test this notion, we substituted all 18 phosphorylation site residues with alanine (ATG13a^{18A}) or aspartate (ATG13a^{18D}) and overexpressed them in *atg13ab* (Figure 5B). ATG13a^{18A} significantly improved the tolerance of the mutant to fixed-C starvation, since the transgenic line *p35S:YFP-ATG13a*^{18A}*/atg13ab* showed delayed senescence compared with *p35S:YFP-ATG13a/atg13ab* (Figure 5, B and C). By contrast, ATG13a^{18D} only partially recovered the sensitivity of *atg13ab* to fixed-C starvation (Figure 5, B and C). These results suggest that dephosphorylation of ATG13a helps plants tolerate carbon deficiency.

The ATG1-ATG13 protein kinase complex is both a regulator and a target of autophagic recycling in Arabidopsis (Suttangkakul et al., 2011). To assess whether the delayed starvation-induced senescence by ATG13a^{18A} did indeed occur due to autophagy induction, we examined the deposition of YFP-ATG13a-labeled autophagic bodies inside the central vacuole. The translocation of YFP-ATG13a^{18A} was much stronger than that of ATG13a and ATG13a^{18D} (Figure 6, A and B). YFP-release assays further confirmed the confocal microscopy observation (Figure 6C).

When autophagy is activated, ATG8 proteins associate with the phospholipid phosphatidylethanolamine (PE) to form ATG8-PE. The amount of ATG8-PE usually correlates with the number of punctate ATG8-positive structures as well as autophagic activity (Chung et al., 2010; Mizushima et al., 2010; Bassham, 2015; Li et al., 2015). To investigate whether the phosphorylation of ATG13a affects ATG8-PE adduct formation, we performed immunoblot analysis. We detected clear ATG8a-PE bands in *atg13ab* and WT, but not in *atg7-3* or *atg5-1*, using our ATG8a-specific antibody (Figure 6D), which is consistent with previous studies (Chung et al., 2010; Suttangkakul et al., 2011). More ATG8a-PE accumulated in *YFP-ATG13a*^{18A}*/atg13ab* plants than the WT, as shown by the enhanced ATG8a-PE/ATG8a ratio (Figure 6E). Although both ATG8a and ATG8a-PE proteins accumulated in *p35S:ATG13a*^{18D}*/atg13ab*, the ATG8a-PE/ATG8a ratio decreased due to the inhibition of autophagy (Figure 6E). These results indicate that the dephosphorylation of up to 18 sites of ATG13a contributes to the regulation of its activity during autophagy.

We next investigated the effects of these 18 residues on the dephosphorylation of ATG13a by performing in vitro assays. Both ATG13a^{18A} and ATG13a^{18D} were less sensitive to λPP and TOPP4-GST than ATG13a (Figure 6F). Meanwhile, a phospho-immunoblotting assay confirmed that TOPP4-RFP-mediated dephosphorylation of YFP-ATG13a^{18A} and YFP-ATG13a^{18D} was significantly inhibited compared to the wild-type protein (Figure 6G). When exposed to fixed-C starvation, the migration caused by dephosphorylation of ATG13a^{18A} and ATG13a^{18D} was difficult to observe (Figure 6H), suggesting these sites are important for maintaining the phosphorylation state of ATG13a. However, the dephosphorylation of ATG13a^{18A} and ATG13a^{18D} was not completely blocked, as determined by immunoblotting with pSer antibody (Figure 6H), implying that other phosphorylation sites exist. Taken together, these results suggest that dephosphorylation of ATG13a at

A Summary of ATG13a phosphorylation peptides identified by LC-MS/MS

Annotated Sequence	Phosphopeptide	Modification Site
241-IITDYVGSPATDPMR-255	IITDYVGsPATDPmR	S248
265-FFPSPGRSVEGHSFTGR-272	FFPsPGRSVEGHSFTGR	S259
	FFPSPGRsVEGHSFTGR	S263
327-TDAFGDNHQLS	TDAFGDNHQLsPPFSPSGSPSTPR	S337
PPFSPSGSPSTPR-350	TDAFGDNHQLSPPFsPSGSPSTPR	S341
	TDAFGDNHQLSPPFSPsGSPSTPR	S343
351-YISGGNSPR-359	yISGGNSPR	Y351
360-INVRPGTAPVTIPSSATLNR-379	INVRPGtAPVTIPSSATLNR	T366
380-YVSSNFSEPGRNPLPPFSPK-399	YVSSNFSEPGRNPLPPFsPK	S397
400-STRRSPSSQDSLPGIALYR-418	sTRRSPSSQDSLPGIALYR	S400
	StRRSPSSQDSLPGIALYR	T401
404-SPSSQDSLPGIALYR-418	sPSSQDSLPGIALYR	S404
	SPsSQDSLPGIALYR	S406
	SPSsQDSLPGIALYR	S407
422-SGESPSGLMNQYPTQK-437	sGESPSGLmNQYPTQK	S422
	SGEsPSGLmNQYPTQK	S425
464-FSGVLSSSDSPR-475	FSGVLSSSDsPR	S473
521-TSSSISQSLPLGR-533	TSSSISQsLPLGR	S528

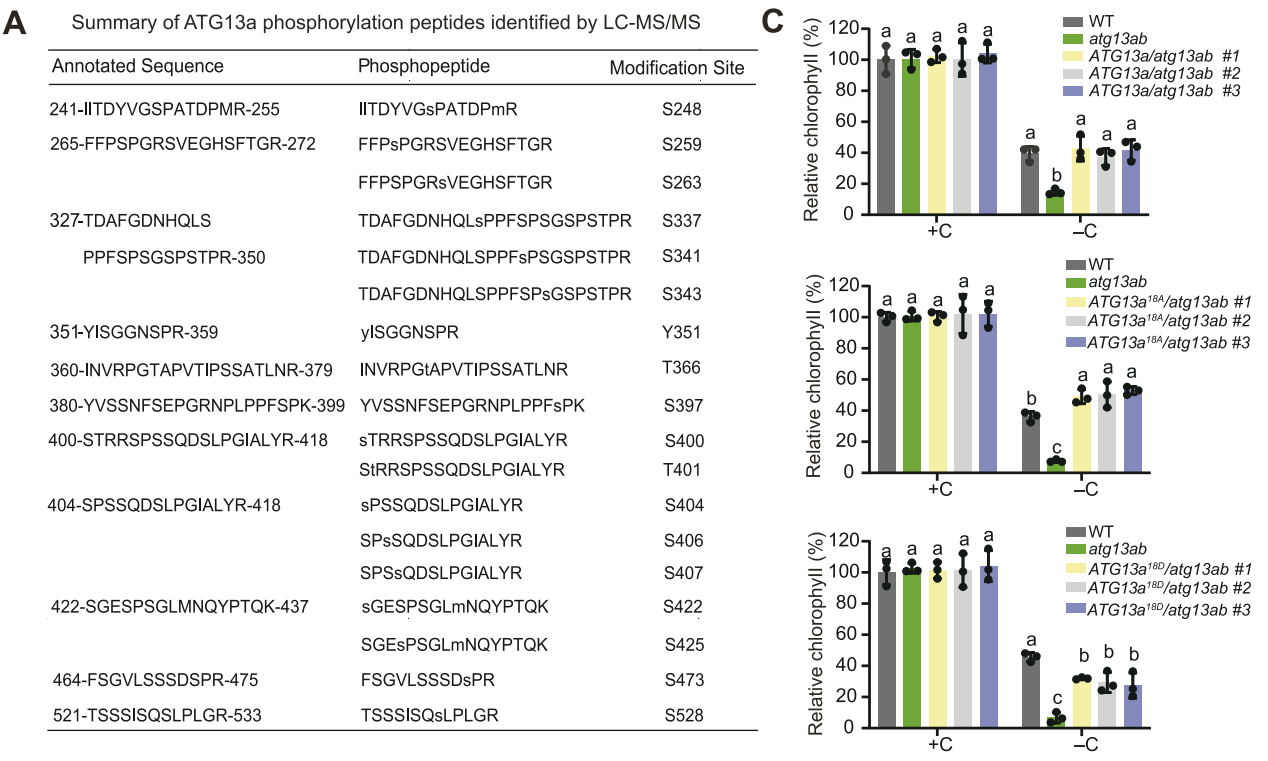

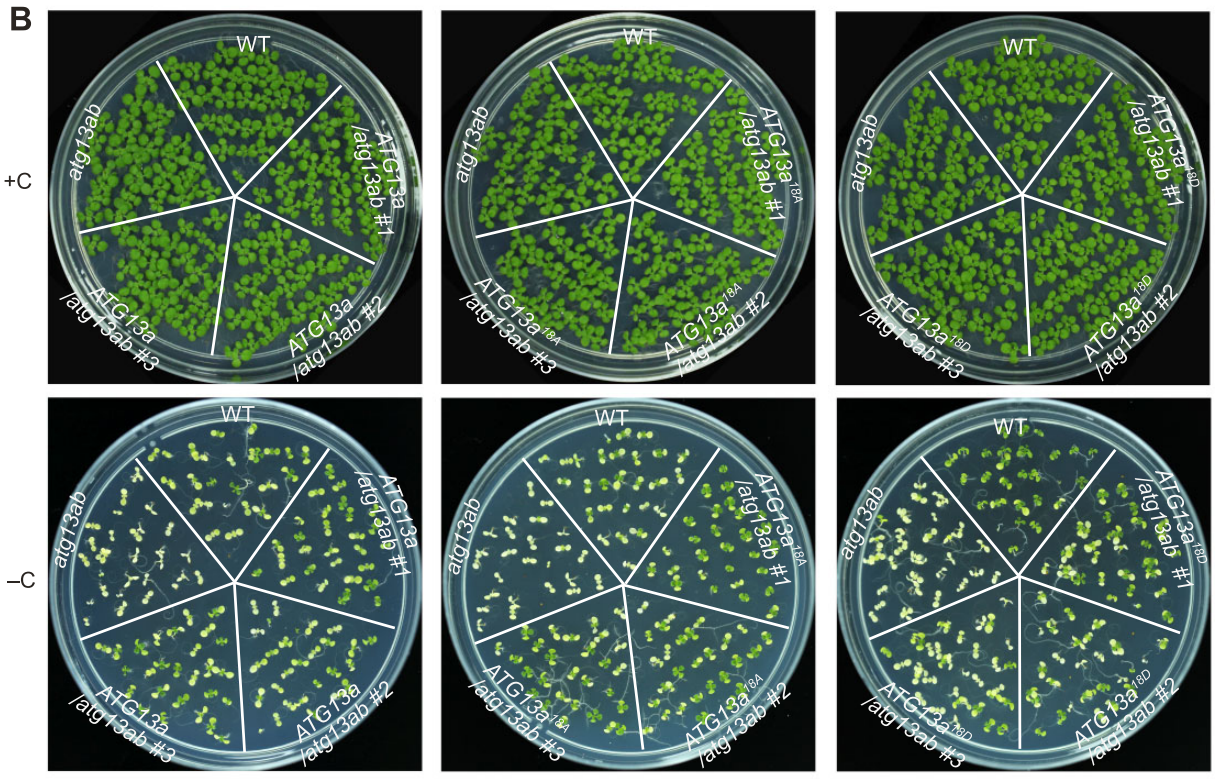

Figure 5 Dephosphorylation of ATG13a enhances plant tolerance to fixed-C starvation. A, Summary of ATG13a phosphorylation sites identified by LC-MS/MS. B, Phenotypes of the transgenic plants *p35S:YFP-ATG13a/atg13ab*, *p35S:YFP-ATG13a^{18A}/atg13ab*, and *p35S:YFP-ATG13a^{18D}/atg13ab* in response to fixed-C starvation. Seedlings were grown on 1/2 MS solid medium with sucrose under LD continuously (+ C) or grown on sucrose-free 1/2 MS solid medium under LD for 7 d, incubated in the dark for 11 d, and allowed to recover for 4 d in LD (−C). C, Relative chlorophyll contents of seedlings shown in (B). Values are means ± SD of three biological replicates. Significant differences were calculated by one-way ANOVA. Different letters above each bar indicate statistically significant differences, as determined by Tukey's multiple testing methods ($P < 0.05$). For each biological replicate, a population of at least 25 plants was examined per genotype.

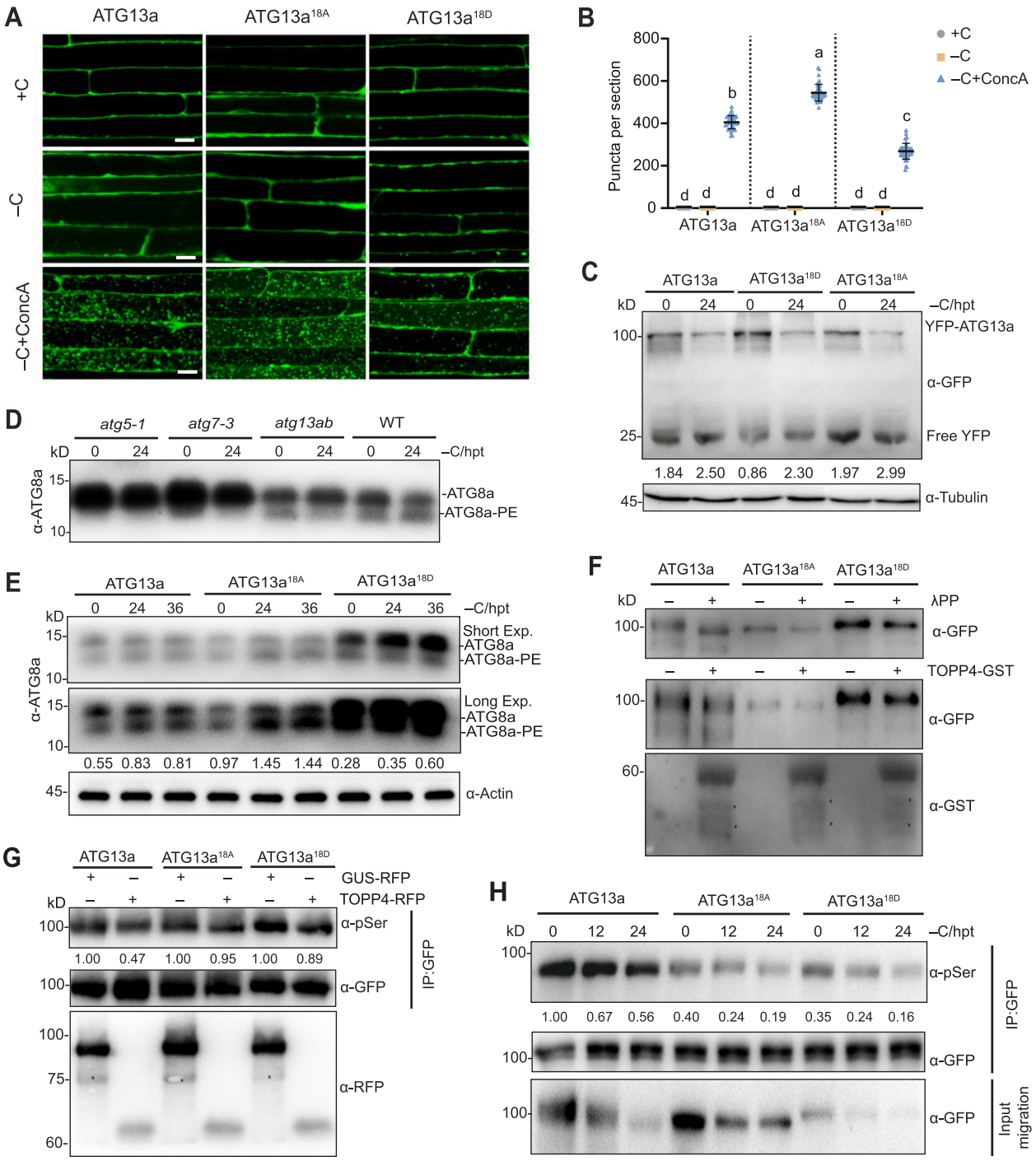

Figure 6 Dephosphorylation of ATG13a enhances fixed-C starvation-induced autophagy. A, Confocal images of YFP-ATG13a, YFP-ATG13a^{18A}, and YFP-ATG13a^{18D} labeled autophagic bodies inside the central vacuoles. *p35S:YFP-ATG13a/atg13ab*, *p35S:YFP-ATG13a^{18A}/atg13ab*, and *p35S:YFP-ATG13a^{18D}/atg13ab* seedlings grown on 1/2 MS medium for 5 d were transferred to +C or −C conditions with or without 0.5 μM ConcA for 12 h. Scale bars, 10 μm. B, Quantification of the number of autophagic bodies shown in (A). Four different images in the root elongation zone were photographed per seedling, and the number of puncta in each image was counted and averaged. A total of 10 seedlings were observed per treatment. Data represent mean ± SD (n = 40), analyzed by one-way ANOVA followed by Tukey's multiple comparison analyses ($P < 0.05$). The center line represents the mean of autophagic bodies. Whiskers represent two SDs. Different letters represent significantly different means. C, Free YFP release from YFP-ATG13a, YFP-ATG13a^{18D}, and YFP-ATG13a^{18A} after fixed-C starvation. *p35S:YFP-ATG13a/atg13ab*, *p35S:YFP-ATG13a^{18D}/atg13ab*, and *p35S:YFP-ATG13a^{18A}/atg13ab* seedlings grown on 1/2 MS medium for 7 d were starved for the indicated time, and total protein extracts were immunoblotted with anti-GFP antibody. Values below each lane represent the ratio of free YFP to YFP fusions, as quantified by ImageJ. hpt, hours post-treatment. D, Immunoblot detecting the ATG8a lipidation level in *atg5-1*, *atg7-3*, *atg13ab*, and WT upon fixed-C starvation. Plants were treated the same as in (C). Membrane fractions were blotted with anti-ATG8a antibody. hpt, hours post-treatment. E, Immunodetection of ATG8a lipidation level in *p35S:YFP-ATG13a/atg13ab*, *p35S:YFP-ATG13a^{18A}/atg13ab*, and *p35S:YFP-ATG13a^{18D}/atg13ab*.

(continued)

multiple sites enhances its function in fixed-C starvation-induced autophagy.

TOPP-controlled ATG13a dephosphorylation promotes the formation of the ATG1a-ATG13a complex

Arabidopsis ATG13a contains a classical ATG13 domain at its N-terminus and an intrinsically disordered region (IDR) at its C-terminus. All 18 phosphorylation sites we identified are located in this IDR (Figure 7A). *Nicotiana benthamiana* transient expression experiments showed that ATG13a localized to the cytoplasm and formed a punctate structure (Figure 7B; Supplemental Figure S16A). When IDR was missing (ATG13a^{n}), ATG13a accumulated in the nucleus, while the IDR alone (ATG13a^{c}) did not alter the localization of ATG13a, suggesting that the IDR is required for the correct subcellular localization of ATG13a (Figure 7B; Supplemental Figure S16A). Moreover, repeated experiments showed that ATG13a^{18D} significantly reduced the formation of puncta in the cytoplasm compared with ATG13a and ATG13a^{18A} (Figure 7, B and C; Supplemental Figure S16A), implying that the phosphorylation state affects ATG13a localization.

We then examined the interaction of ATG1a and ATG13a. A Y2H assay showed that IDR, excluding the N-terminus, mediated the interaction between ATG1a and ATG13a (Figure 7D). BiFC and Co-IP experiments further confirmed this result (Figure 7E; Supplemental Figure S16B). Given that IDR contains multiple phosphorylation sites, we analyzed whether the phosphorylation state of ATG13a affects its interaction with ATG1a. Y2H and BiFC showed that both ATG13a^{18A} and ATG13a^{18D} bind to ATG1a (Figure 7, D and E). However, an in vivo Co-IP assay revealed that ATG13a^{18D} significantly reduced their interaction (Supplemental Figure S16C).

To further explore the ATG1a–ATG13a interaction during fixed-C starvation, we performed Co-IP experiments. Under normal growth conditions, a basal interaction between ATG1a and ATG13a was detected. After treatment with fixed-C starvation, this affinity significantly increased (Figure 7, F and G). Interestingly, the phospho-dead form ATG13a^{18A} strongly enhanced the recruitment of ATG1a, while the phospho-mimic ATG13a^{18D} reduced their interaction (Figure 7H). Since ATG13a was hyperphosphorylated in *topp-7m-1* (Figure 4, G–I), it is reasonable to assume that the ATG1a-ATG13a association was impaired in the mutant. To test this hypothesis, we performed a similar Co-IP experiment. The interaction of ATG1a and ATG13a was notably reduced in *topp-7m-1* under fixed-C starvation (Figure 7, I and J). Based on these results, we conclude that the formation of the ATG1a-ATG13a complex is regulated by the phosphorylation state of ATG13a and that this process is tightly controlled by TOPP.

TOPP-controlled dephosphorylation of ATG13a boosts ATG1a phosphorylation

As the ATG1a-ATG13a interaction was impaired in *topp-7m-1*, we set out to determine whether TOPP directly regulates ATG1a. Y2H analysis showed that TOPP4 physically interacted with ATG1a (Figure 8A). BiFC and Co-IP assays confirmed this interaction in vivo (Figure 8, B and C). In addition to TOPP4, TOPP1 also bound to ATG1a (Figure 8, A and B). TOPP4 interacted with the ATG1a homologous proteins ATG1b and ATG1c both in vitro and in vivo, but not with the homologous protein ATG1t (Supplemental Figure S17, A–C).

To investigate whether TOPP dephosphorylates ATG1a in vitro, we used *atg7-3*, a mutant in which ATG1a is hyperphosphorylated following fixed-C/N starvation (Li et al., 2014), as the material (Figure 8D). The phosphorylated state of ATG1a could be removed by protein phosphatase λPP. However, the hyperphosphorylated ATG1a could not be directly dephosphorylated by TOPP4 (Figure 8E). When YFP-ATG1a was coexpressed with TOPP4-RFP in *N. benthamiana*, there were no significant changes in phosphorylation signal compared with GUS-RFP (Figure 8F). Finally, to further test the effect of TOPP4 on ATG1a in Arabidopsis, we overexpressed *TOPP4* in the *atg7-3* background. Interestingly, repeated experiments showed that *TOPP4* obviously promoted the phosphorylation of ATG1a during autophagy (Figure 8G; Supplemental Figure S17D), and the dephosphorylated form of ATG13a continuously appeared in *TOPP4-GFP/atg7-3*, like in the *TOPP* overexpression lines (Figure 8H; Supplemental Figure S12, D–F). However, the enhanced phosphorylation of ATG1a was not observed in the *atg13ab* mutant (Figure 8I). Therefore, the TOPP-mediated promotion of ATG1a phosphorylation may depend on ATG13a.

Figure 6 (Continued)

Seedlings were treated the same as in (C). The ATG8a-PE/ATG8a ratio, representing autophagy activity, is shown below the blots. hpt, hours post-treatment. F, Dephosphorylation of ATG13a^{18A} and ATG13a^{18D} by λ phosphatase and TOPP4-GST in vitro. *p35S:YFP-ATG13a/atg13ab*, *p35S:YFP-ATG13a^{18A}/atg13ab*, and *p35S:YFP-ATG13a^{18D}/atg13ab* seedlings were collected from 1/2 MS medium. Total proteins were immunoprecipitated with GFP magnetic beads, and the purified beads were treated with λPP or TOPP4-GST and subjected to immunoblot analysis with anti-GFP antibody. Asterisks represent nonspecific bands. G, Dephosphorylation of ATG13a, ATG13a^{18A}, and ATG13a^{18D} by TOPP4 in *N. benthamiana*. TOPP4-RFP together with YFP-ATG13a, YFP-ATG13a^{18A}, or YFP-ATG13a^{18D} was transiently coexpressed in *N. benthamiana* leaves. α-GFP IP was used to remove the background. Phosphorylation of ATG13a was examined by immunoblotting with anti-pSer. Numbers below the blots represent the relative abundance of phosphorylated ATG13a. Asterisks represent non-specific bands. GUS-RFP was used as a negative control. H, Effects of phospho-dead (18A) and phospho-mimic (18D) of ATG13a on their dephosphorylation under fixed-C starvation in Arabidopsis. *atg13ab* seedlings expressing YFP-tagged ATG13a, ATG13a^{18A}, and ATG13a^{18D} grown on 1/2 MS medium for 7 d were treated with fixed-C starvation for the indicated time. hpt, hours post-treatment.

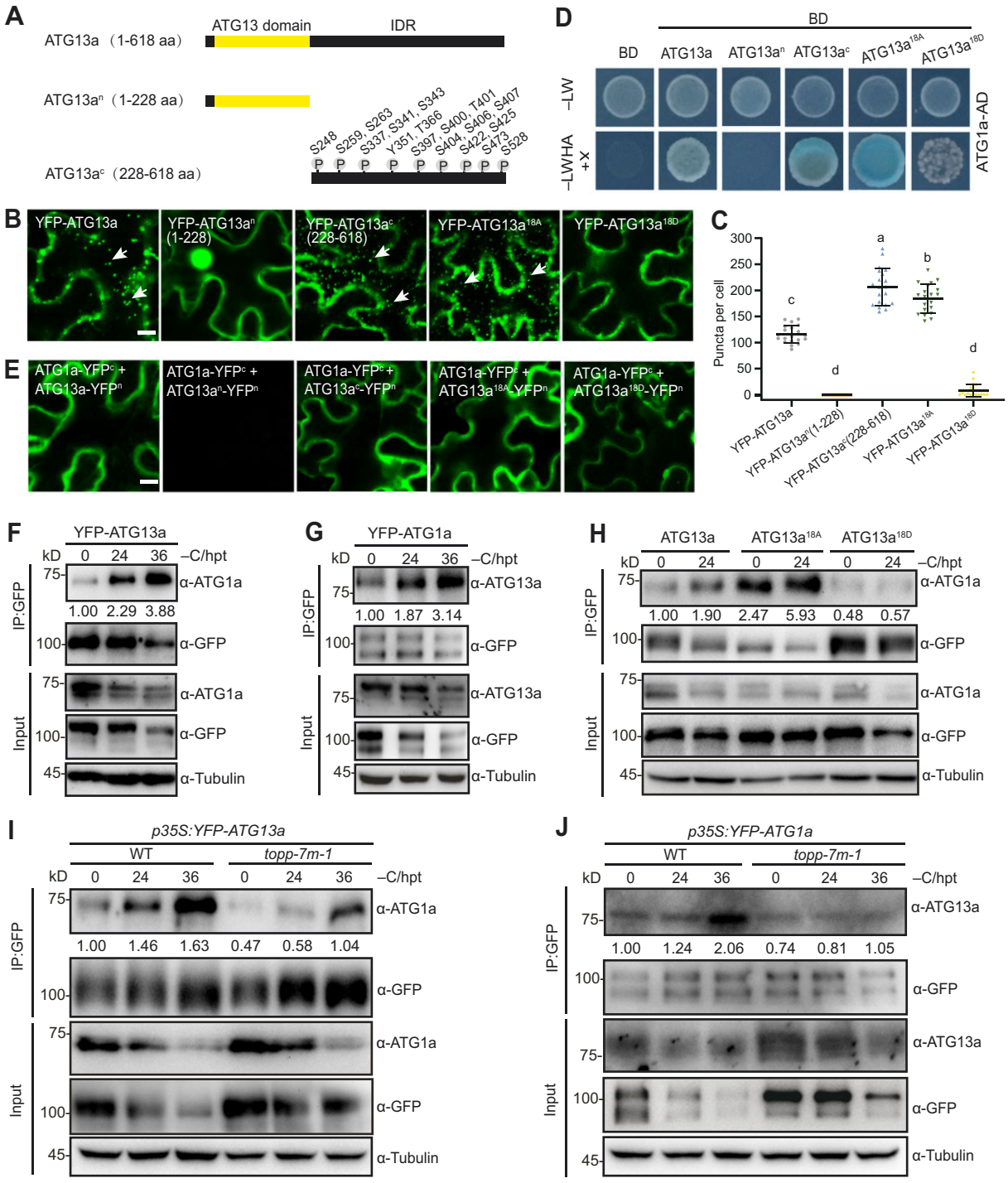

Figure 7 TOPP-controlled dephosphorylation of ATG13a promotes the formation of the ATG1a-ATG13a complex. A, Illustration of the ATG13a domain. The numbers indicate the positions of the amino acids in the constructs. ATG13a indicates full-length ATG13a, ATG13a^{n} indicates the N-terminal fragment of ATG13a, and ATG13a^{c} indicates the C-terminal fragment of ATG13a. B, Subcellular localization of ATG13a, ATG13a^{n}, ATG13a^{c}, ATG13a^{18A}, and ATG13a^{18D} in *N. benthamiana* epidermal cells. Arrows indicate ATG13a puncta in the cytoplasm. Scale bar, 50 μm. C, Quantification of the puncta structures shown in (B). Data represent the average number of punctate structures per cell, $n = 20$, analyzed by one-way ANOVA followed by Tukey's multiple comparison analyses ($P < 0.05$). The center line represents the mean of puncta structures. Whiskers represent two SDs. Different letters represent significantly different means. D, Y2H analysis of the interaction between ATG1a and full-length, truncated, or mutated ATG13a. –LW, SD medium lacking Trp and Leu; –LWHA + X, SD medium lacking Trp, Leu, His, and Ade; X, X-α-gal. Empty BD was used as control. E, BiFC analysis showing the interaction between ATG1a and full-length, truncated, or mutated ATG13a in *N. benthamiana*. Scale bar, 50 μm. F and G, ATG1a and ATG13a interaction upon fixed-C starvation. *p35S:YFP-ATG13a*/WT or *p35S:YFP-ATG1a*/WT seedlings grown on 1/2 MS medium for 7 d were treated with fixed-C starvation for the indicated time. Total proteins were immunoprecipitated with anti-GFP beads, and the bound protein was detected by anti-ATG1a or anti-ATG13a antibody. Values below each lane represent the ratio of

(continued)

Discussion

PP1 is a major class of the PPP family of Ser/Thr protein phosphatases that is ubiquitously distributed throughout eukaryotes (Farkas et al., 2007; Uhrig et al., 2013). In mammals, PP1 determines the fate of cardiomyocytes during hypoxia/reoxygenation by regulating the dephosphorylation of ATG16L1 during autophagy (Song et al., 2015). This implies that TOPP may play a role in plant autophagy.

In this study, we determined that the *TOPP* dominant-negative mutant *topp4-1* displayed an autophagy-deficient phenotype, which is consistent with the phenotype of the well-known autophagy mutant *atg7-3* under fixed-C starvation. However, the homozygous single mutants of *TOPP* did not show similar phenotypes, nor did the *topp-2m*, *topp-3m*, *topp-4m*, *topp-5m*, or *topp-6m* mutants. The septuple mutant (*topp-7m*) and octuple mutant (*topp-8m*) were sensitive to fixed-C starvation, like *atg13ab*. Although we recovered only five (*TOPP1*, *TOPP4*, *TOPP5*, *TOPP8*, and *TOPP9*) alleles of the *topp1/4/5/6/7/8/9* (*topp-7m-1*) mutant, and additional *TOPP* genes (such as *TOPP3*) were not mutated in the multiple knockouts, we believe that the above phenotypes observed in the *topp-7m* and *topp-8m* mutants were caused by *TOPP* mutations and that the higher-order mutant *topp-9m* must also have the same phenotype as *topp4-1*. We noticed that *TOPP7* failed to fully complement *topp-7m-1*, although TOPP7 interacted with ATG13a in a BiFC experiment, suggesting that TOPP7 is not a major TOPP that regulates ATG13a, or perhaps it functions indirectly in this process by targeting other factors.

Autophagic bodies could be observed upon ConcA treatment (Suttangkakul et al., 2011; Qi et al., 2017; Huang et al., 2019; Liu et al., 2020). We determined that TOPP entered the vacuoles in the form of puncta in the presence of ConcA. However, these TOPP-labeled dots did not completely overlap with GFP-ATG8e, and TOPP4 did not degrade as quickly as GFP-ATG8e under fixed-C starvation conditions. In a previous study, we demonstrated that TOPP4 is required for the endocytic trafficking of PIN1 in pavement cells (Guo et al., 2015). Therefore, these TOPP-puncta in vacuoles might also contain other non-autophagosome acidic vesicles, as ConcA is a vacuolar ATPase inhibitor that prevents the trafficking of acidic vesicle (either endosomes or autophagosomes) and inhibits vacuolar degradation activity (Dröse et al., 1993; Huss et al., 2002; Dettmer et al., 2006). On the other hand, ATG8 also plays a non-autophagic function in plant senescence through the endosomal pathway (Jia et al., 2019). Nonetheless, the colocalization of ATG8 and TOPP indicates that TOPP is involved in autophagy.

To determine whether TOPP functions in plant autophagy via a mechanism similar to that observed in mammals, we first examined the relationship between TOPP and ATG16. Unfortunately, we did not detect any interaction between TOPP and ATG16 (Supplemental Figure S10, C and D). Therefore, TOPP may regulate plant autophagy via a different mechanism in plants. The ATG1-ATG13 complex plays an essential role in initiating autophagy, sensing nutritional status signals, recruiting downstream ATG proteins, and governing autophagosome formation (Suttangkakul et al., 2011; Li et al., 2014; Huang et al., 2019; Qi et al., 2019; Wang and Hou, 2022). However, the functional phosphorylation sites of ATG13a have not been verified, and its associated protein phosphatase is unclear. Here, we determined that TOPP is the phosphatase that directly targets ATG13a. There are two ATG13s (ATG13a and ATG13b) in Arabidopsis, which function redundantly in regulating autophagy (Suttangkakul et al., 2011). Surprisingly, no TOPP isoforms interacted with ATG13b in yeast or *N. benthamiana*, which is similar to the previous findings for KIN10 and TRAF1a/b (Chen et al., 2017; Qi et al., 2019). Bioinformatic analysis revealed sequence differences between ATG13a and ATG13b. Both proteins contain large segments of IDR in the sequence (Wang and Hou, 2022). It is reasonable to assume that this flexible sequence triggers differences in the conformations and functions of ATG13a and ATG13b. In addition, the 18 phosphorylation sites of ATG13a are not completely conserved in ATG13b, suggesting that the regulatory mechanisms of ATG13a and ATG13b phosphorylation might differ. However, upon fixed-C starvation, the ATG13b-TOPP4 interaction was observed in Arabidopsis, implying that either *ATG13a* or *ATG13b* is sufficient to supply ATG13 protein when autophagy is induced and that TOPP may also target ATG13b.

In this study, 18 crucial phosphorylation sites of ATG13a were identified. Even though Ser248 was previously considered to be a potential carbon/nitrogen-responsive phosphorylation site of ATG13a (Li et al., 2020), the substitution of the four conserved serine residues (including Ser248) among the 18 phosphorylation sites did not significantly affect the function of ATG13a, suggesting that these four residues are not the key phosphorylation sites of ATG13a. However, when all 18 phosphorylation sites were mutated to A simultaneously, the function of ATG13a was markedly enhanced and autophagy was activated. This multi-site phospho-

Figure 7 (Continued)
ATG1a to ATG13a or ATG13a to ATG1a, as quantified by ImageJ. The gray value of two bands of ATG1a was calculated as a whole in (G). hpt, hours post-treatment. H, Coimmunoprecipitation of ATG13a, ATG13a^{18A}, and ATG^{18D} with ATG1a upon fixed-C starvation. *p35S:YFP-ATG13a/atg13ab*, *p35S:YFP-ATG13a^{18A}/atg13ab*, and *p35S:YFP-ATG13a^{18D}/atg13ab* seedlings were treated the same as in (F) and (G). Values represent the ratio of ATG1a to AG13a or mutated ATG13a. hpt, hours post-treatment. I and J, The interaction of ATG1a and ATG13a in *topp-7m-1* upon fixed-C starvation. *p35S:YFP-ATG13a*/WT, *p35S:YFP-ATG13a/topp-7m-1*, *p35S:YFP-ATG1a*/WT, and *p35S:YFP-ATG1a/topp-7m-1* seedlings were treated the same as in (F) and (G). Values below each lane represent the ratio of ATG1a to ATG13a or ATG13a to ATG1a, as quantified by ImageJ. The gray value of two bands of ATG1a was calculated as a whole in (J). All protein experiments were repeated 3 times with similar results. hpt, hours post-treatment.

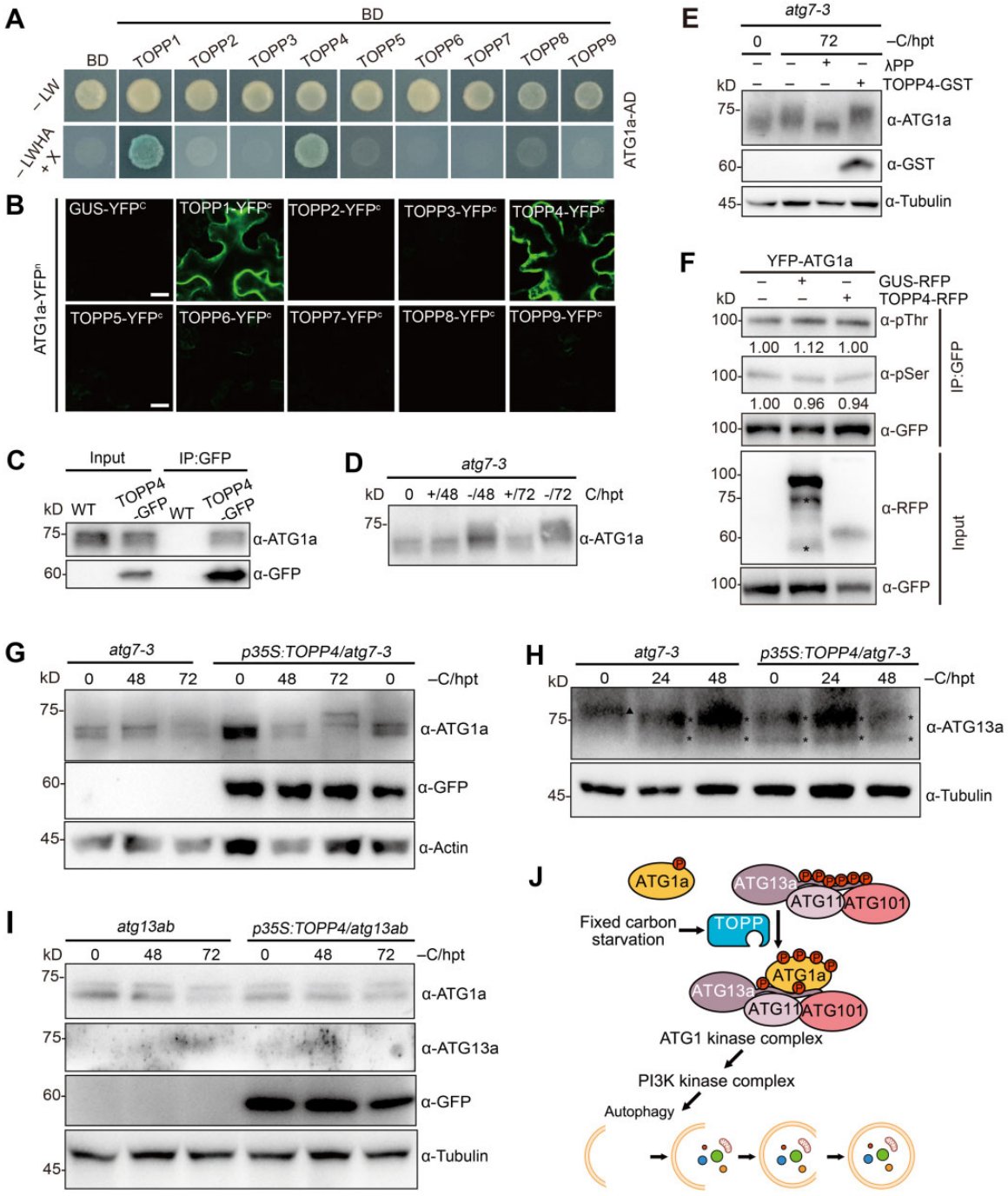

Figure 8 TOPP-controlled dephosphorylation of ATG13a boosts ATG1a phosphorylation. A, Interaction of TOPP with ATG1a in a Y2H assay. −LW, SD medium lacking Trp and Leu; −LWHA + X, SD medium lacking Trp, Leu, His, and Ade; X, X-α-gal. Empty BD was used as control. B, BiFC assay showing the interaction between TOPP and ATG1a in *N. benthamiana*. β-glucuronidase (GUS) was used as a non-interacting control. Scale bars, 100 μm. C, Coimmunoprecipitation of TOPP4 with ATG1a. Total proteins were extracted from 1-week-old WT and *p35S:TOPP4-GFP*/WT seedlings, immunoprecipitated with GFP magnetic beads, and analyzed using anti-ATG1a antibody. D, Phosphorylation of ATG1a in *atg7-3* under fixed-C starvation. *atg7-3* seedlings grown on 1/2 MS solid medium for 7 d were transferred to + C or −C conditions for the indicated time. Total proteins were extracted from the samples and immunoblotted with anti-ATG1a antibody. hpt, hours post-treatment. E and F, TOPP4 cannot dephosphorylate ATG1a. One-week-old *atg7-3* seedlings were treated for 72 h under fixed-C starvation. Total proteins were extracted from the samples and treated with λPP or TOPP4-GST, followed by immunoblot analysis with anti-ATG1a antibody. hpt, hours post-treatment (E).TOPP4-RFP together with YFP-ATG1a was transiently coexpressed in *N. benthamiana* leaves. Phosphorylation of ATG1a was conducted by pSer and pThr antibodies immunoblotting. Numbers below the blots represent the relative abundance of phosphorylated ATG1a. Asterisks represent nonspecific bands. GUS-RFP was used as a control (F). G, TOPP4 promotes phosphorylation of ATG1a in *atg7-3*. *atg7-3* and *p35S:TOPP4-GFP*/*atg7-3* seedlings were grown on 1/2 MS medium for 7 d and treated with fixed-C starvation for different periods of time. Total proteins were extracted from the samples and immunoblotted with anti-ATG1a antibody. hpt, hours post-treatment. H, ATG13a is hypo-phosphorylated in *p35S:TOPP4-GFP*/*atg7-*

(continued)

regulation of ATG13a suggests that the number of sites available for phosphorylation is a more important determinant of ATG13a activity than the exact locations of those sites. This multi-site phosphorylation regulatory mechanism has been reported in plants (Smertenko et al., 2006; Ni et al., 2013; Hardwick and Philpott, 2015). Similarly, in yeast, Atg13 is a hyper-phosphorylated protein that contains at least 51 phosphorylation sites, and dephosphorylation of Atg13 at eight serine residues is sufficient for the induction of autophagy (Kamada et al., 2010; Fujioka et al., 2014; Yeasmin et al., 2016; Memisoglu and Haber, 2019). It is also worth noting that three potential phosphorylation sites of ATG13a, Thr251, Ser268, and Ser558 (Van Leene et al., 2019), were not identified in our study, suggesting that there are additional phosphorylation sites in ATG13a that require further investigation. Indeed, at least 37 phosphorylation sites may exist in Arabidopsis ATG13a according to bioinformatics analysis (Supplemental Figure S16D; Wang and Hou, 2022). Additionally, the presence of Tyr351 indicates that other types of protein phosphatases, such as PTP (protein tyrosine phosphatase), might also be involved in the dephosphorylation of ATG13a. Thus, compared to yeast, the regulation of ATG13a phosphorylation during plant autophagy is more complicated. How these phosphorylation sites of ATG13a respond to different environmental conditions and nutrient deficiency requires further study.

Arabidopsis ATG13a, one of the core components of the ATG1-ATG13 complex, was structurally divided into an N-terminal ATG13 domain and a C-terminal IDR region which contains a large number of phosphorylation sites. We found that the IDR was required for the localization of ATG13a in the punctate structures of the cytoplasm. Furthermore, ATG13a-puncta formation was dependent on the dephosphorylation of ATG13a. Interestingly, these puncta-like signals were specifically generated by ATG13a and ATG13b, but not by other ATG proteins such as ATG8e, ATG1a, ATG1b, or ATG1c (Supplemental Figure S16, E and F), although these ATGs also include the classic IDR (Supplemental Figure S16G). Yeast Atg13 also contains an IDR containing 51 phosphorylation sites at its C-terminus, which is essential for the pre-autophagosomal structure (PAS) localization of Atg13 itself (Jao et al., 2013; Suzuki et al., 2015; Yamamoto et al., 2016), suggesting that the IDR of ATG13 is conserved in different organisms. Yeast PAS is a liquid-like condensate of Atgs in which the Atg1 complex undergoes phase separation to form liquid droplets; this process is dynamically controlled by Atg13 phosphorylation (Fujioka et al., 2020). However, the exact nature of these ATG13a/b-puncta in Arabidopsis remains unknown, since it is not clear whether the PAS exists in plants. Future work should investigate whether these ATG13a/b-puncta in plants are the result of a similar type of phase separation like in yeast.

We found that ATG13a was quickly dephosphorylated, while ATG1a was phosphorylated upon fixed-C starvation. Moreover, fixed-C starvation or phospho-dead ATG13a ($ATG13a^{18A}$) enhanced the ATG1a-ATG13a interaction. Therefore, the regulatory mode of the ATG1-ATG13 complex in Arabidopsis is similar to that of yeast (Cebollero and Reggiori, 2009; Kamada et al., 2010; Fujioka et al., 2014). By contrast, in mammalian cells, both ULK1 and ATG13 are dephosphorylated when starvation triggers autophagy. The binding of ULK1 and ATG13 is not regulated by nutritional conditions (Mizushima, 2010; Yang and Klionsky, 2010). On the contrary, in fruit fly (*Drosophila melanogaster*), ATG13 is highly phosphorylated, whereas ATG1 is dephosphorylated when autophagy is induced by starvation. The *Drosophila* ATG1 and ATG13 interaction is stable under both fed and starved conditions (Chang and Neufeld, 2010). Hence, although the Atg1-Atg13 complex is conserved in eukaryotes, it has complicated regulatory mechanisms in different species with regard to the switching of its phosphorylation state and formation during autophagy. Besides, in yeast, the phosphorylation of Atg13 not only affects its binding to Atg1 but also alters its interaction with Atg17 (Fujioka et al., 2014; Memisoglu et al., 2019). While Arabidopsis appears to be missing a separate canonical ATG17 protein, instead, an ATG11/17 hybrid was detected (Li et al., 2014). Therefore, the phosphorylation status of ATG13 might affect its interaction with ATG11 in Arabidopsis.

Interestingly, TOPP4 could not dephosphorylate ATG1a, although they interacted with each other directly. In addition, the phosphorylation of ATG1a increased when *TOPP4* was overexpressed in *atg7-3*. We propose that accumulated ATG13a is first dephosphorylated by TOPP4, resulting in the formation of hypo-phosphorylated ATG13a, which binds to ATG1a. ATG1a is then auto-phosphorylated or phosphorylated by other kinases via an unknown mechanism.

Collectively, our observations present strong evidence that TOPP is a positive regulator of fixed-C starvation-induced autophagy in Arabidopsis. Under nutrient-rich conditions, ATG13a is highly phosphorylated, reducing its affinity for the ATG1a kinase. After fixed-C starvation, an unknown component then activates TOPP to dephosphorylate ATG13a, promoting ATG1a-ATG13a complex formation and ATG1a phosphorylation (Figure 8J). In summary, our

Figure 8 (Continued)

3. Seedlings were treated the same as in (G). Total proteins were extracted from the samples and immunoblotted with anti-ATG13a antibody. The triangle indicates the hyper-phosphorylated form of ATG13a, and the asterisks represent the hypo-phosphorylated form of ATG13a. hpt, hours post-treatment. I, The role of TOPP4 in promoting the phosphorylation of ATG1a is dependent on ATG13. *atg13ab* and *p35S:TOPP4-GFP/atg13ab* seedlings were treated the same as in (G). Total proteins were extracted from the samples and immunoblotted with anti-ATG1a antibody. hpt, hours post-treatment. J, Proposed model for the role of TOPP in regulating autophagy in Arabidopsis. ATG13a is kept in a hyper-phosphorylated state under nutrient-rich conditions. Upon fixed carbon starvation, TOPP contributes to the dephosphorylation of ATG13a, forming a tight ATG1a-ATG13a complex. ATG1a is then phosphorylated and autophagy is induced.

findings illustrate how ATG13a is dephosphorylated after the induction of autophagy by fixed-C starvation and uncover the key phosphatase that regulates this process in plants.

Materials and methods

Plant materials and growth conditions

All materials used in this work were in the *A. thaliana* accession Columbia (Col-0) background. The *topp1-1* (SALK_057537), *topp2* (GK_187C10_014623/CS305848), *topp6* (SALK_093747), *topp7* (SALK_023073), *topp8-1/aun2-1* (SALK_137888), *topp9/aun1-1* (SALK_045433C), *atg5-1* (SAIL_129_B07) and *atg7-3* (SAIL_11_H07) mutants were obtained from the Arabidopsis Biological Resource Center (ABRC). *topp4-3* (SALK_098324) was obtained from Prof. Yong Ding (University of Science and Technology of China). The dominant-negative mutant *topp4-1* has been described (Qin et al., 2014). The *topp3*, *topp5*, *topp-2m*, *topp-3m*, *topp-4m*, *topp-5m*, *topp-6m*, *topp-7m*, and *topp-8m* mutants were generated as shown in Supplemental Data Set S1. *atg13ab* (SALK_044831) was obtained from Prof. Fa Qiang Li (South China Agricultural University; Suttangkakul et al., 2011). The transgenic lines *pATG8e:GFP-ATG8e*/Col-0 and *pUBQ10:ATG13b-HA*/Col-0 were obtained from Prof. Shi Xiao (Sun Yat-sen University; Huang et al., 2018). Other stable expression transgenic plants were generated as described in Supplemental Data Set S1. All plants obtained by CRISPR-Cas9-mediated gene editing were screened on hygromycin. After separation of the *Cas9* gene from the mutants, non-hygromycin-resistant seeds were used for the experiments.

Arabidopsis seeds were surface-sterilized, vernalized at 4°C for 2–3 d, and germinated on 1/2 MS medium at 22°C under a long day (LD) photoperiod (16 h light/8 h dark) with illumination at ∼100 μmol m^{-2} s^{-1} using bulbs (cat. no.WT5-LED14 14W; FSL). After 1 week, the seedlings were transferred to soil for further growth. *Nicotiana benthamiana* was grown under LD conditions same as Arabidopsis. One-month-old *N. benthamiana* plants were used for the transient expression assays.

Fixed-carbon starvation treatment

The effects of fixed-carbon starvation on plant growth and survival were determined as described (Suttangkakul et al., 2011). Briefly, for +C, seedlings were grown on 1/2 MS solid medium with sucrose under LD for 20 d. For −C, seedlings were grown on sucrose-free 1/2 MS solid medium under LD for 1 week, transferred to the dark for 9–10 d, and allowed to recover for 3–4 d in LD. To detect protein expression, seedlings grown under LD on 1/2 MS solid medium for 1 week were transferred to −C liquid medium for different periods of time.

Measurement of relative chlorophyll contents

Seedlings were homogenized in phosphate buffer (50 mmol/L, pH 6.8), 50 μL plant homogenate was added with 450 μL 95% (v/v) ethanol and incubating at 4°C in the dark for 30 min. Supernatants were separated from tissue debris by centrifugation at 14,000 rpm at 4°C for 10 min. Absorbances of the supernatant at 652 nm were measured. The relative chlorophyll content was calculated as described previously (Qi et al., 2017; Yang et al., 2020).

Plasmid construction

Most plasmids used in this study were generated using a Gateway Cloning Kit (Thermo Fisher Scientific) according to the manufacturer's instructions. Briefly, full-length coding sequence fragments of *TOPPs* or *ATGs* were amplified and inserted into pDONR-Zeo via the Gateway BP Clonase I reaction. Sequence-confirmed coding sequences were then subcloned into destination vectors. To generate vectors harboring mutated versions of *ATG13a*, primers carrying mutated bases were designed, and PCR was performed using pDONR-Zeo carrying sequence-confirmed *ATG13a* as the template. The PCR products were digested with DpnI at 37°C for 5 h and used to transform *E. coli*. To generate CRISPR-Cas9 vectors, the Golden Gate method was used to construct a vector expressing one or two gRNA-specific targets as described (Xing et al., 2014).

Y2H assay

To test direct protein-protein interactions by Y2H, pairwise AD and BD were cotransformed into yeast strain Y2H gold (Clontech). Cells transformed with both plasmids were selected after growth 2 d at 30°C on synthetic dropout medium lacking leucine and tryptophan. Protein-protein interactions were then identified by growing the yeast for 2 d at 30°C on synthetic dropout medium lacking adenine, leucine, tryptophan, and histidine and containing 20 mg/mL X-α-gal. To confirm interactions, single colony was diluted in sterile H_2O to an OD600 of 0.1, and 10 μL was spotted onto both types of selective medium and again grown for 2 d at 30°C.

Bimolecular fluorescence complementation (BiFC) and transient protein expression in *N. benthamiana*

In planta protein-protein interactions were assayed by bimolecular fluorescence complementation in *N. benthamiana* leaves. The plasmids were introduced into *Agrobacterium tumefaciens* strain GV3101. Overnight cultures were resuspended in 5 mL infiltration buffer (0.15 M acetosyringone dilute in DMSO; 0.01 M MES, pH 7.5; 0.01 M $MgCl_2$), incubated at room temperature for 4 h in the dark, and used for direct infiltration of 4- to 6-week-old *N. benthamiana* leaves. Leaf sections of approximately 2 mm × 2 mm excised 36–48 h after infiltration were visualized under a Nikon A1+ confocal laser scanning microscope using 20× objectives. Transient protein expression was conducted as described for BiFC.

Drug treatment and confocal laser scanning microscopy

For concanavalin A (ConcA) treatment, Arabidopsis seedlings expressing GFP or YFP reporters were grown on 1/2 MS medium for 5 d, transferred to sucrose-free liquid

medium with or without 0.5 μM ConcA, and grown for 12 h in the dark. For calyculin A (CL-A) treatment, 5-day-old seedlings grown on 1/2 MS agar medium were preincubated with or without 0.5 μM CL-A in 1/2 MS liquid medium for 60 min, transferred to sucrose-deficient liquid medium with 0.5 μM ConcA, and incubated for an additional 12 h in the dark. Following incubation, the GFP/YFP labeled autophagic bodies in the roots were visualized under a Nikon A1 + confocal laser scanning microscope using 40× water objectives. Excitation was performed at 488 nm and 543 nm, and emission was collected at 500–530 nm or 565–615 nm for GFP and RFP signals, respectively. Identical settings were used to image *N. benthamiana* leaf sections subjected to *A. tumefaciens*-mediated infiltration as described above.

Protein isolation and immunoblot analysis

For protein extraction, Arabidopsis samples were ground and homogenized in ice-cold extraction buffer (10 mM HEPES, pH 7.5; 100 mM NaCl; 1 mM EDTA pH 8.0; 10% Glycerol; 0.5% Triton X-100; 1 × cocktail). Samples were incubated on ice for 10–15 min and centrifuged at 4°C for 10 min at 12,000 *g*. The supernatant was used for electrophoresis. For immunoblot analysis, total proteins were subjected to SDS-PAGE and electrophoretically transferred to a polyvinylidene fluoride membrane (Immobilon-P; Millipore). For the ATG8a assay, total proteins were separated by SDS-PAGE in the presence of 6 M urea. Antibodies used in protein blotting analysis are listed in Supplemental Data Set S1. For dephosphorylation experiments, samples were subjected to 8% SDS-PAGE at 80 V for 3 h and electrophoretically transferred to PVDF membrane for 1 h at 100 V.

Recombinant protein expression and pull-down

To express recombinant proteins in prokaryotic cells, the coding sequences of the TOPPs were cloned into the pGEX 4T-3 (GST tag) or pET28a (HIS tag) vector and transformed into *E. coli* strain *Rosetta*. GST-tagged proteins were purified with Glutathione Sepharose 4B beads (10250335, GE Healthcare) following the manufacturer's instructions. HIS tagged proteins were purified with BeaverBeads™ IDA-Nickel (17B026101, Beaver) following the manufacturer's instructions. Protein concentration was determined using a BCA protein assay kit (Solarbio, PC0021).

The in vitro pull-down assay was performed as described (Guo et al., 2015). ATG13a-MBP and ATG13b-MBP were purified using PurKine™ MBP-Tag Dextrin Resin 6FF (BMR20206, Abbkine). MBP beads containing ATG13a-MBP and ATG13b-MBP were incubated with purified GST or TOPP4-GST protein at 4°C for 2 h with gentle shaking. After washing several times with wash buffer, the proteins were detected by immunoblotting with anti-GST antibody.

p-Nitrophenyl phosphate (pNPP) phosphatase activity assay

Phosphatase activity assays were performed as described previously (Templeton et al., 2011; Hou et al., 2016). The general substrate p-nitrophenyl phosphate (pNPP, Sigma, N3002) was used to measure the phosphatase activity of TOPP4. Reactions were performed in assay buffer (50 mM Tris-HCl, pH 7.5, 2 mM $MnCl_2$, 1 mM EDTA, 0.5% β-mercaptoethanol, 2 mg/mL BSA and 50 mM pNPP) with an increasing gradient of TOPP4-GST recombinant protein at 37°C for 1 h. After incubation, the reactions were quenched with 5 volumes of 0.5 M EDTA. The hydrolysis of pNPP was measured by following the absorbance at 405 nm (A405).

Coimmunoprecipitation (Co-IP)

For Co-IP in Arabidopsis, 1-week-old WT or transgenic seedlings overexpressing *TOPP4-GFP* were ground in liquid nitrogen and homogenized in ice-cold IP buffer (10 mM HEPES, pH 7.5; 100 mM NaCl; 1 mM EDTA pH 8.0; 10% glycerol; 0.5% Triton X-100; 1 × cocktail). The samples were incubated on ice for 10–15 min and centrifuged at 4°C for 10 min at 12,000 *g*. The supernatant was then incubated with GFP magnetic beads (D153-11, MBL) for 2 h at 4°C to immunoprecipitate the target protein. The beads were collected and washed with cold IP buffer 3–5 times.

Co-IP in *N. benthamiana* was performed as described, with minor modifications (Li et al., 2017). The p35S:TOPP4-FLAG and p35S:YFP-ATGs constructs were infiltrated into *N. benthamiana* via the *Agrobacterium*-mediated method. After 48 h, total proteins were extracted from the samples with IP buffer (50 mM Tris-HCl, pH 7.5; 150 mM NaCl; 5 mM dithiothreitol; 1% Triton X-100; 2% NP40 and 1 × cocktail), followed by incubation with anti-FLAG magnetic beads (M185-11R, MBL) for 2 h. The beads were washed 6–8 times with washing buffer (50 mM Tris-HCl, pH 7.5; 150 mM NaCl; 1% Triton X-100; 2% NP40). The immunoprecipitated proteins were analyzed by SDS-PAGE and immunoblotted with anti-GFP antibody.

λ protein phosphatase treatment and dephosphorylation assay in vivo

Transgenic plant *p35S:YFP-ATG13a/atg13ab* was grown on 1/2 MS medium for 7 d and homogenized in 2:1 (volume to fresh weight) IP buffer as described above. The target protein was immunoprecipitated at 4°C for 2 h. The GFP-beads were washed 3 times with cold IP buffer, followed by three washes with reaction buffer (50 mM HEPES, pH 7.5; 100 mM NaCl; 5 mM DTT; 0.01% Brij35; 1 mM $MnCl_2$; 10 mM Na_2EDTA and 0.1% Triton X-100; supplemented with 1 mM phenylmethylsulfonyl fluoride and 1 × cocktail). The beads were then suspended in fresh 50 μL reaction buffer, incubated with λ protein phosphatase (40 units/μL; P0753S, New England Biolabs) or recombinant TOPP4-GST/HIS for 1 h at 30°C. The reactions were quenched by adding an equal volume of 2 × SDS-PAGE sample buffer and heating to 95°C for 5 min. To examine the dephosphorylation of ATG1a in *atg7-3*, total proteins were directly extracted from the samples in 1.25:1 reaction buffer (volume to fresh weight). Clarified extracts were then incubated with λ protein phosphatase or TOPP4-GST as described above.

Mass spectrometry analysis

To prepare samples for mass spectrometry analysis, at least 2 g *p35S:YFP-ATG13a/atg13ab* seedlings grown on 1/2 MS medium for 1 week were collected. YFP-ATG13a was immunoprecipitated as described above, 50 μL of concentrated immunoprecipitated was separated by SDS-PAGE. Gels were stained with G-250, and the YFP-ATG13a band was excised. In-gel tryptic digestion and mass spectrometry analysis were performed as described (Sun et al., 2021). The samples were analyzed on an Orbitrap Fusion Lumos mass spectrometer (Thermo Fisher Scientific) connected to an EASY-nLC 1200 system. Proteome Discoverer Daemon 2.2 software (Thermo Fisher Scientific) was used for data analysis.

RT-qPCR analysis

RNA was extracted from the samples using a Total RNA kit (OMEGA) following the manufacturer's instructions. 5 × PrimeScript™ RT Master Mix (TAKARA) was used to synthesize cDNA. RT-qPCR analysis was performed using SYBR Premix Ex Taq II (TaKaRa) and a Stepone PCR instrument. *Ubiquitin10* (*UBQ10*) was used as a reference gene. The gene-specific primers used for RT-qPCR are listed in Supplemental Data Set S1.

Sequence alignment

Predicted full-length protein sequences were obtained from UniProt (https://www.uniprot.org/). Sequences were aligned with Clustal Omega (https://www.ebi.ac.uk/Tools/msa/clustalo/).

Statistical analysis

SPSS statistics 22.0 software (IBM) was used for the statistical analysis of the data. The data are expressed as the mean ± SD and were subjected to a two-tailed Student's *t*-test or one-way analysis of variance (ANOVA) Tukey's multiple range tests ($P < 0.05$). Details of statistical analysis are provided in Supplemental Data Set S4.

Accession numbers

Sequence data for the genes used in this study can be found in The Arabidopsis Information Resource (www.arabidopsis.org) under the following accession numbers: *TOPP1* (AT2G29400), *TOPP2* (AT5G59160), *TOPP3* (AT1G64040), *TOPP4* (AT2G39840), *TOPP5* (AT3G46820), *TOPP6* (AT4G11240), *TOPP7* (AT5G43380), *TOPP8* (AT5G27840), *TOPP9* (AT3G05580), *ATG1a* (AT3G61960), *ATG1b* (AT3G53930), *ATG1c* (AT2G37840), *ATG1t* (AT1G49180), *ATG8a* (AT4G21980), *ATG8e* (AT2G45170), *ATG13a* (AT3G49590), *ATG13b* (AT3G18770), *ATG16* (AT5G50230), *ATG5* (AT5G17290), *ATG7* (AT5G45900), *ATG12a* (AT1G54210), *SINAT6* (At3g13672), *KIN10* (AT3G01090).

Supplemental data

The following materials are available in the online version of this article.

Supplemental Figure S1. Dominant-negative mutant *topp4-1* and loss function mutants *topp-7m-2* and *topp-7m-3* are hypersensitive to fixed-C starvation.

Supplemental Figure S2. Transcription of *TOPPs* upon fixed-C starvation.

Supplemental Figure S3. Identification and generation of *topp* mutants.

Supplemental Figure S4. *topp* single mutants exhibit no obvious phenotype upon fixed-C starvation.

Supplemental Figure S5. *topp-2m*, *topp-3m*, *topp-4m*, *topp-5m*, and *topp-6m* show no obvious phenotype compared to WT upon fixed-C starvation.

Supplemental Figure S6. The sensitivity of *topp-7m-1* to fixed-C starvation is recovered by *TOPP1*, *TOPP5*, *TOPP8*, and *TOPP9* expression.

Supplemental Figure S7. Overexpression of *TOPP1* and *TOPP5* enhances plant tolerance to fixed-C starvation.

Supplemental Figure S8. Autophagic flux is affected by TOPP phosphatase activity.

Supplemental Figure S9. The expression of *ATGs* in WT and *topp-7m-1* upon fixed-C starvation.

Supplemental Figure S10. Interactions between TOPPs and ATG13a, ATG13b, or ATG16.

Supplemental Figure S11. Subcellular localization of TOPP upon fixed-C starvation depends on autophagy.

Supplemental Figure S12. ATG13a is dephosphorylated upon fixed-C starvation.

Supplemental Figure S13. Amino acid sequence alignment of ATG13a and ATG13b in *Arabidopsis thaliana*.

Supplemental Figure S14. Conservation analysis of 18 phosphorylation sites of ATG13a in different species.

Supplemental Figure S15. Substitution of Ser248, Ser343, Ser397, and Ser473 has no effect on the function of ATG13a in response to fixed-C starvation.

Supplemental Figure S16. Interaction between different domains of ATG1a and ATG13a; possible phosphorylation sites of ATG13; subcellular localization of ATG1a/1b/1c, ATG8e, ATG13a/13b; and IDR prediction of ATG1a/1b/1c, ATG8e, ATG13a/13b.

Supplemental Figure S17. TOPP4 interacts with ATG1a/1b/1c and promotes ATG1a phosphorylation.

Supplemental Table S1. Identification of ATG13a peptides in GFP-tagged TOPP4 immunoprecipitation product.

Supplemental Table S2 List of ATG13a homologous proteins.

Supplemental Table S3. Analysis of the phosphorylation of ATG13a in WT and *topp4-1* by iTRAQ quantitative phosphoproteomics.

Supplemental Data Set S1. Oligonucleotide primers, mutants, and transgenic lines, constructs, and antibodies used in this study.

Supplemental Data Set S2. Details of phosphorylated ATG13a peptides identified by LC-MS/MS.

Supplemental Data Set S3. Quantitative iTRAQ-based proteomic analysis of phosphoprotein ATG13a in WT and *topp4-1*.

Supplemental Data Set S4. Quantitative raw data of relative chlorophyll content, RT-qPCR, confocal images, and immunoblotting.

Acknowledgments

We thank Prof. FaQiang Li (South China Agricultural University) for *atg13ab* mutant, Prof. QiJun Chen (China Agricultural University) for pCBC-DT1T2 and pHEE401 vector. We are grateful to Liang Peng, LiPing Guan, and YaHu Gao (Core Facility at Life Science Research, Lanzhou University) for technical assistance.

Funding

This work was supported by the National Natural Science Foundation of China (32170340).

Conflict of interest statement. The authors declare no competing interests.

References

Alers S, Loffler AS, Paasch F, Dieterle AM, Keppeler H, Lauber K, Campbell DG, Fehrenbacher B, Schaller M, Wesselborg S, et al. (2011) Atg13 and FIP200 act independently of Ulk1 and Ulk2 in autophagy induction. Autophagy **7**: 1424–1433

Bassham DC (2015) Methods for analysis of autophagy in plants. Methods **75**: 181–188

Bheri M, Mahiwal S, Sanyal SK, Pandey GK (2021) Plant protein phosphatases: what do we know about their mechanism of action? FEBS J **288**: 756–785

Bradai M, Amorim-Silva V, Belgaroui N, Esteban Del Valle A, Chabouté ME, Schmit AC, Lozano-Duran R, Botella MA, Hanin M, Ebel C (2021) Wheat type one protein phosphatase participates in the brassinosteroid control of root growth via activation of BES1. Int J Mol Sci **22**: 10424.

Bradai M, Mahjoubi H, Chini A, Chaboute ME, Hanin M, Ebel C (2018) Genome wide identification of wheat and *Brachypodium* type one protein phosphatases and functional characterization of durum wheat TdPP1a. PLoS One **13**: e0191272.

Cebollero E, Reggiori F (2009) Regulation of autophagy in yeast *Saccharomyces cerevisiae*. Biochim Biophys Acta **1793**: 1413–1421

Chang Y-Y, Neufeld TP (2009) An Atg1/Atg13 complex with multiple roles in TOR-mediated autophagy regulation. Mol Biol Cell **20**: 2004–2014

Chang Y-Y, Neufeld TP (2010) Autophagy takes flight in *Drosophila*. FEBS Lett **584**: 1342–1349

Chen L, Su Z-Z, Huang L, Xia F-N, Qi H, Xie L-J, Xiao S, Chen Q-F (2017) The AMP-activated protein kinase KIN10 is involved in the regulation of autophagy in Arabidopsis. Front Plant Sci **8**: 1201

Chung T, Phillips AR, Vierstra RD (2010) ATG8 lipidation and ATG8-mediated autophagy in Arabidopsis require ATG12 expressed from the differentially controlled ATG12A and ATG12B loci. Plant J **62**: 483–493

Dettmer J, Hong-Hermesdorf A, Stierhof YD, Schumacher K (2006) Vacuolar H^+-ATPase activity is required for endocytic and secretory trafficking in Arabidopsis. Plant Cell **18**: 715–730

Doelling JH, Walker JM, Friedman EM, Thompson AR, Vierstra RD (2002) The APG8/12-activating enzyme APG7 is required for proper nutrient recycling and senescence in *Arabidopsis thaliana*. J Biol Chem **277**: 33105–33114

Dröse S, Bindseil KU, Bowman EJ, Siebers A, Zeeck A, Altendorf K (1993) Inhibitory effect of modified bafilomycins and concanamycins on P- and V-type adenosinetriphosphatases. Biochemistry **32**: 3902–3906

Farkas I, Dombradi V, Miskei M, Szabados L, Koncz C (2007) Arabidopsis PPP family of serine/threonine phosphatases. Trends Plant Sci **12**: 169–176

Franck CM, Westermann J, Burssner S, Lentz R, Lituiev DS, Boisson-Dernier A (2018) The protein phosphatases ATUNIS1 and ATUNIS2 regulate cell wall integrity in tip-growing cells. Plant Cell **30**: 1906–1923

Fujioka Y, Alam JM, Noshiro D, Mouri K, Ando T, Okada Y, May AI, Knorr RL, Suzuki K, Ohsumi Y, et al. (2020) Phase separation organizes the site of autophagosome formation. Nature **578**: 301–305

Fujioka Y, Suzuki SW, Yamamoto H, Kondo-Kakuta C, Kimura Y, Hirano H, Akada R, Inagaki F, Ohsumi Y, Noda NN (2014) Structural basis of starvation-induced assembly of the autophagy initiation complex. Nat Struct Mol Biol **21**: 513.

Guo X, Qin Q, Yan J, Niu Y, Huang B, Guan L, Li Y, Ren D, Li J, Hou S (2015) TYPE-ONE PROTEIN PHOSPHATASE4 regulates pavement cell interdigitation by modulating PIN-FORMED1 polarity and trafficking in Arabidopsis. Plant Physiol **167**: 1058–1075

Hanaoka H, Noda T, Shirano Y, Kato T, Hayashi H, Shibata D, Tabata S, Ohsumi Y (2002) Leaf senescence and starvation-induced chlorosis are accelerated by the disruption of an Arabidopsis autophagy gene. Plant Physiol **129**: 1181–1193

Hardwick LJ, Philpott A (2015) Multi-site phosphorylation regulates NeuroD4 activity during primary neurogenesis: a conserved mechanism amongst proneural proteins. Neural Dev **10**: 15.

Hoehenwarter W, Thomas M, Nukarinen E, Egelhofer V, Röhrig H, Weckwerth W, Conrath U, Beckers GJ (2013) Identification of novel in vivo MAP kinase substrates in *Arabidopsis thaliana* through use of tandem metal oxide affinity chromatography. Mol Cell Proteomics **12**: 369–380

Hou YJ, Zhu Y, Wang P, Zhao Y, Xie S, Batelli G, Wang B, Duan CG, Wang X, Xing L, et al. (2016) Type one protein phosphatase 1 and its regulatory protein inhibitor 2 negatively regulate ABA signaling. PLoS Genet **12**: e1005835.

Hu Y, Ding Y, Cai B, Qin X, Wu J, Yuan M, Wan S, Zhao Y, Xin XF (2022) Bacterial effectors manipulate plant abscisic acid signaling for creation of an aqueous apoplast. Cell Host Microbe **30**: 518–529

Huang L, Yu L-J, Zhang X, Fan B, Wang F-Z, Dai Y-S, Qi H, Zhou Y, Xie L-J, Xiao S (2018) Autophagy regulates glucose-mediated root meristem activity by modulating ROS production in Arabidopsis. Autophagy **15**: 407–422

Huang X, Zheng C, Liu F, Yang C, Zheng P, Lu X, Tian J, Chung T, Otegui MS, Xiao S, et al. (2019) Genetic analyses of the Arabidopsis ATG1 kinase complex reveal both kinase dependent and independent autophagic routes during fixed-carbon starvation. Plant Cell **31**: 2973–2995

Huss M, Ingenhorst G, König S, Gassel M, Dröse S, Zeeck A, Altendorf K, Wieczorek H (2002) Concanamycin A, the specific inhibitor of V-ATPases, binds to the V(o) subunit c. J Biol Chem **277**: 40544–40548

Jao CC, Ragusa MJ, Stanley RE, Hurley JH (2013) A HORMA domain in Atg13 mediates PI3-kinase recruitment in autophagy. Proc Natl Acad Sci USA **110**: 5486–5491

Jia M, Liu X, Xue H, Wu Y, Shi L, Wang R, Chen Y, Xu N, Zhao J, Shao J, et al. (2019) Noncanonical ATG8-ABS3 interaction controls senescence in plants. Nat Plants **5**: 212–224

Kabeya Y, Kamada Y, Baba M, Takikawa H, Sasaki M, Ohsumi Y (2005) Atg17 functions in cooperation with Atg1 and Atg13 in yeast autophagy. Mol Biol Cell **16**: 2544–2553

Kamada Y, Funakoshi T, Shintani T, Nagano K, Ohsumi M, Ohsumi Y (2000) Tor-mediated induction of autophagy via an Apg1 protein kinase complex. J Cell Biol **150**: 1507–1513

Kamada Y, Yoshino K, Kondo C, Kawamata T, Oshiro N, Yonezawa K, Ohsumi Y (2010) Tor directly controls the Atg1 kinase complex to regulate autophagy. Mol Cell Biol **30**: 1049–1058

Liao Y-D, Lin K-H, Chen C-C, Chiang C-M (2016) *Oryza sativa* protein phosphatase 1a (OsPP1a) involved in salt stress tolerance in transgenic rice. Mol Breeding **36**: 22.

Li F, Chung T, Pennington JG, Federico ML, Kaeppler HF, Kaeppler SM, Otegui MS, Vierstra RD (2015) Autophagic recycling plays a central role in maize nitrogen remobilization. Plant Cell **27**: 1389–1408

Li F, Chung T, Vierstra RD (2014) AUTOPHAGY-RELATED11 plays a critical role in general autophagy and senescence-induced mitophagy in Arabidopsis. Plant Cell **26**: 788–807

Li H, Ding Y, Shi Y, Zhang X, Zhang S, Gong Z, Yang S (2017) MPK3- and MPK6-mediated ICE1 phosphorylation negatively regulates ICE1 stability and freezing tolerance in Arabidopsis. Dev Cell **43**: 630–642

Li X, Liu Q, Feng H, Deng J, Zhang R, Wen J, Dong J, Wang T (2019) Dehydrin MtCAS31 promotes autophagic degradation under drought stress. Autophagy **16**: 862–877

Li X, Sanagi M, Lu Y, Nomura Y, Stolze SC, Yasuda S, Saijo Y, Schulze WX, Feil R, Stitt M, et al. (2020) Protein phosphorylation dynamics under carbon/nitrogen-nutrient stress and identification of a cell death-related receptor-like kinase in Arabidopsis. Front Plant Sci **11**: 377.

Liu Y, BasshamDC (2012) Autophagy: pathways for self-eating in plant cells. Annu Rev Plant Biol **63**: 215–237

Liu F, Hu W, Li F, Marshall RS, Zarza X, Munnik T, Vierstra RD (2020) AUTOPHAGY-RELATED14 and its associated phosphatidylinositol 3-kinase complex promotes autophagy in Arabidopsis. Plant Cell **32**: 3939–3960

Liu Y, Yan J, Qin Q, Zhang J, Chen Y, Zhao L, He K, Hou S (2019) Type one protein phosphatases (TOPPs) contribute to the plant defense response in Arabidopsis. J Integr Plant Biol **62**: 360–377

Marshall RS, Vierstra RD (2018) Autophagy: the master of bulk and selective recycling. Annu Rev Plant Biol **69**: 173–208

Memisoglu G, Eapen VV, Yang Y, Klionsky DJ, Haber JE (2019) PP2C phosphatases promote autophagy by dephosphorylation of the Atg1 complex. Proc Natl Acad Sci USA **116**: 1613–1620

Memisoglu G, Haber JE (2019) Dephosphorylation of the Atg1 kinase complex by type 2C protein phosphatases. Mol Cell Oncol **6**: 1588658.

Michaeli S, Galili G, Genschik P, Fernie AR, Avin-Wittenberg T (2016) Autophagy in plants-what's new on the menu? Trends Plant Sci **21**: 134–144

Mizushima N (2010) The role of the Atg1/ULK1 complex in autophagy regulation. Curr Opin Cell Biol **22**: 132–139

Mizushima N, Yoshimori T, Levine B (2010) Methods in mammalian autophagy research. Cell **140**: 313–326

Ni W, Xu SL, Chalkley RJ, Pham TN, Guan S, Maltby DA, Burlingame AL, Wang ZY, Quail PH (2013) Multisite light-induced phosphorylation of the transcription factor PIF3 is necessary for both its rapid degradation and concomitant negative feedback modulation of photoreceptor phyB levels in Arabidopsis. Plant Cell **25**: 2679–2698

Phillips AR, Suttangkakul A, Vierstra RD (2008) The ATG12-conjugating enzyme ATG10 is essential for autophagic vesicle formation in *Arabidopsis thaliana*. Genetics **178**: 1339–1353

Pu Y, Luo X, Bassham DC (2017) TOR-dependent and-independent pathways regulate autophagy in *Arabidopsis thaliana*. Front Plant Sci **8**: 1204.

Puente C, Hendrickson RC, Jiang X (2016) Nutrient-regulated phosphorylation of ATG13 inhibits starvation-induced autophagy. J Biol Chem **291**: 6026–6035

Wong P-M, Feng Y, Wang J, Shi R, Jiang X (2015) Regulation of autophagy by coordinated action of mTORC1 and protein phosphatase 2A. Nat Commun **6**: 8048.

Qi H, Li J, Xia FN, Chen JY, Lei X, Han MQ, Xie LJ, Zhou QM, Xiao S (2019) Arabidopsis SINAT proteins control autophagy by mediating ubiquitylation and degradation of ATG13. Plant Cell **32**: 263–284

Qin Q, Wang W, Guo X, Yue J, Huang Y, Xu X, Li J, Hou S (2014) Arabidopsis DELLA protein degradation is controlled by a type-one protein phosphatase, TOPP4. PLoS Genet **10**: e1004464.

Qi H, Xia F-N, Xie L-J, Yu L-J, Chen Q-F, Zhuang X-H, Wang Q, Li F, Jiang L, Xie Q, et al. (2017) TRAF family proteins regulate autophagy dynamics by modulating AUTOPHAGY PROTEIN6 stability in Arabidopsis. Plant Cell **29**: 890–911

Ren C, Liu J, Gong Q (2014) Functions of autophagy in plant carbon and nitrogen metabolism. Front Plant Sci **5**: 301.

Rodriguez E, Chevalier J, Olsen J, Ansbøl J, Kapousidou V, Zuo Z, Svenning S, Loefke C, Koemeda S, Drozdowskyj PS (2020) Autophagy mediates temporary reprogramming and dedifferentiation in plant somatic cells. EMBO J **39**: e103315.

Schumacher K, Liu Y, Bassham DC (2010) TOR is a negative regulator of autophagy in *Arabidopsis thaliana*. PLoS One **5**: e11883.

Sedaghatmehr M, Thirumalaikumar VP, Kamranfar I, Marmagne A, Masclaux-Daubresse C, Balazadeh S (2019) A regulatory role of autophagy for resetting the memory of heat stress in plants. Plant Cell Environ **42**: 1054–1064

Smertenko AP, Chang HY, Sonobe S, Fenyk SI, Weingartner M, Bögre L, Hussey PJ (2006) Control of the AtMAP65-1 interaction with microtubules through the cell cycle. J Cell Sci **119**: 3227–3237

Son O, Kim S, Kim D, Hur Y-S, Kim J, Cheon C-I (2018) Involvement of TOR signaling motif in the regulation of plant autophagy. Biochem Biophys Res Commun **501**: 643–647

Song H, Pu J, Wang L, Wu L, Xiao J, Liu Q, Chen J, Zhang M, Liu Y, Ni M (2015) ATG16L1 phosphorylation is oppositely regulated by CSNK2/casein kinase 2 and PPP1/protein phosphatase 1 which determines the fate of cardiomyocytes during hypoxia/reoxygenation. Autophagy **11**: 1308–1325

Soto-Burgos J, Bassham DC (2017) SnRK1 activates autophagy via the TOR signaling pathway in *Arabidopsis thaliana*. PLoS One **12**: e0182591.

Stephan JS, Yeh Y-Y, Ramachandran V, Deminoff SJ, Herman PK (2009) The Tor and PKA signaling pathways independently target the Atg1/Atg13 protein kinase complex to control autophagy. Proc Natl Acad Sci USA **106**: 17049–17054

Stubbs MD, Tran HT, Atwell AJ, Smith CS, Olson D, Moorhead GB (2001) Purification and properties of *Arabidopsis thaliana* type 1 protein phosphatase (PP1). Biochim Biophys Acta **1550**: 52–63

Sun D, Fang X, Xiao C, Ma Z, Huang X, Su J, Li J, Wang J, Wang S, Luan S, et al. (2021) Kinase SnRK1.1 regulates nitrate channel SLAH3 engaged in nitrate-dependent alleviation of ammonium toxicity. Plant Physiol **186**: 731–749

Suttangkakul A, Li F, Chung T, Vierstra RD (2011) The ATG1/ATG13 protein kinase complex is both a regulator and a target of autophagic recycling in Arabidopsis. Plant Cell **23**: 3761–3779

Suzuki K, Kubota Y, Sekito T, Ohsumi Y (2007) Hierarchy of Atg proteins in pre-autophagosomal structure organization. Genes Cells **12**: 209–218

Suzuki K, Ohsumi Y (2010) Current knowledge of the pre-autophagosomal structure (PAS). FEBS Lett **584**: 1280–1286

Suzuki SW, Yamamoto H, Oikawa Y, Kondo-Kakuta C, Kimura Y, Hirano H, Ohsumi Y (2015) Atg13 HORMA domain recruits Atg9 vesicles during autophagosome formation. Proc Natl Acad Sci USA **112**: 3350–3355

Takahashi K, Hayashi K, Kinoshita T (2012) Auxin activates the plasma membrane H^+-ATPase by phosphorylation during hypocotyl elongation in Arabidopsis. Plant Physiol **159**: 632–641

Templeton GW, Nimick M, Morrice N, Campbell D, Goudreault M, Gingras AC, Takemiya A, Shimazaki K, Moorhead GB (2011) Identification and characterization of AtI-2, an Arabidopsis homologue of an ancient protein phosphatase 1 (PP1) regulatory subunit. Biochem J **435**: 73–83

Thompson AR, Doelling JH, Suttangkakul A, Vierstra RD (2005) Autophagic nutrient recycling in Arabidopsis directed by the ATG8 and ATG12 conjugation pathways. Plant Physiol **138**: 2097–2110

Uhrig RG, Labandera A-M, Moorhead GB (2013) Arabidopsis PPP family of serine/threonine protein phosphatases: many targets but few engines. Trends Plant Sci **18**: 505–513

Van Leene J, Han C, Gadeyne A, Eeckhout D, Matthijs C, Cannoot B, De Winne N, Persiau G, Van De Slijke E, Van de Cotte B (2019) Capturing the phosphorylation and protein interaction landscape of the plant TOR kinase. Nat Plants **5**: 316–327

Wang S, Guo J, Zhang Y, Guo Y, Ji W (2021) Genome-wide characterization and expression analysis of TOPP-type protein phosphatases in soybean (*Glycine max L.*) reveal the role of GmTOPP13 in drought tolerance. Genes Genomics **43**: 783–796

Wang Q, Hou S (2022) The emerging roles of ATG1/ATG13 kinase complex in plants. J Plant Physiol **271**: 153653.

Wang P, Pleskot R, Zang J, Winkler J, Wang J, Yperman K, Zhang T, Wang K, Gong J, Guan Y, et al. (2019) Plant AtEH/Pan1 proteins drive autophagosome formation at ER-PM contact sites with actin and endocytic machinery. Nat Commun **10**: 5132

Wang P, Richardson C, Hawes C, Hussey PJ (2016) Arabidopsis NAP1 regulates the formation of autophagosomes. Curr Biol **26**: 2060–2069

Wright AJ, Knight H, Knight MR (2002) Mechanically stimulated TCH3 gene expression in Arabidopsis involves protein phosphorylation and EIN6 downstream of calcium. Plant Physiol **128**: 1402–1409

Xiao S, Gao W, Chen Q-F, Chan S-W, Zheng S-X, Ma J, Wang M, Welti R, Chye M-L (2010) Overexpression of Arabidopsis acyl-CoA binding protein ACBP3 promotes starvation-induced and age-dependent leaf senescence. Plant Cell **22**: 1463–1482

Xie Y, Kang R, Sun X, Zhong M, Huang J, Klionsky DJ, Tang D (2015) Posttranslational modification of autophagy-related proteins in macroautophagy. Autophagy **11**: 28–45

Xing H-L, Dong L, Wang Z-P, Zhang H-Y, Han C-Y, Liu B, Wang X-C, Chen Q-J (2014) A CRISPR/Cas9 toolkit for multiplex genome editing in plants. BMC Plant Bio **14**: 327

Yamamoto H, Fujioka Y, Suzuki SW, Noshiro D, Suzuki H, Kondo-Kakuta C, Kimura Y, Hirano H, Ando T, Noda NN (2016) The intrinsically disordered protein Atg13 mediates supramolecular assembly of autophagy initiation complexes. Dev Cell **38**: 86–99

Yan J, Liu Y, Huang X, Li L, Hu Z, Zhang J, Qin Q, Yan L, He K, Wang Y, et al. (2019) An unreported NB-LRR protein SUT1 is required for the autoimmune response mediated by type one protein phosphatase 4 mutation (topp4-1) in Arabidopsis. Plant J **100**: 357–373

Yang Z, Klionsky DJ (2010) Mammalian autophagy: core molecular machinery and signaling regulation. Curr Opin Cell Biol **22**: 124–131

Yang C, Shen W, Yang L, Sun Y, Li X, Lai M, Wei J, Wang C, Xu Y, Li F (2020) HY5-HDA9 module transcriptionally regulates plant autophagy in response to light-to-dark conversion and nitrogen starvation. Mol Plant **13**: 515–531

Yeasmin AM, Waliullah TM, Kondo A, Kaneko A, Koike N, Ushimaru T (2016) Orchestrated action of PP2A antagonizes Atg13 phosphorylation and promotes autophagy after the inactivation of TORC1. PLoS One **11**: e0166636

Yoshimoto K, Hanaoka H, Sato S, Kato T, Tabata S, Noda T, Ohsumi Y (2004) Processing of ATG8s, ubiquitin-like proteins, and their deconjugation by ATG4s are essential for plant autophagy. Plant Cell **16**: 2967–2983

Yue J, Qin Q, Meng S, Jing H, Gou X, Li J, Hou S (2016) TOPP4 regulates the stability of PHYTOCHROME INTERACTING FACTOR5 during photomorphogenesis in Arabidopsis. Plant Physiol **170**: 1381–1397

Zhang J, Qin Q, Nan X, Guo Z, Liu Y, Jadoon S, Chen Y, Zhao L, Yan L, Hou S (2020) Role of protein phosphatase 1 regulatory subunit 3 (PP1R3) in mediating abscisic acid response. Plant Physiol **184**: 1317–1332

Zhao P, Zhou X-M, Zhao L-L, Cheung AY, Sun M-X (2020) Autophagy-mediated compartmental cytoplasmic deletion is essential for tobacco pollen germination and male fertility. Autophagy **16**: 2180–2192